Correspondence to:
M. S. Petro,
mspetro@nmhu.edu

Vertical Axis Rotation Across the Eastern Mono Basin and West-Central Walker Lane Revealed by Paleomagnetic Data From the Jack Springs Tuff

M. S. Petronis[1] [ID]**, P. J. Zebrowski[1], S. F. Shields[1], C. J. Pluhar[2], and J. R. Lindeman[2]**

[1]Environmental Geology, Natural Resources Management Department, New Mexico Highlands University, Las Vegas, New Mexico, USA, [2]Department of Earth and Environmental Sciences, California State University, Fresno, Fresno, California, USA

Abstract The mid-Miocene Jack Springs Tuff (JST) outcrops from the Bodie Hills of eastern California into the western Mina Deflection, Nevada. Distal outcrops of the JST occur northwest of Mono Lake, CA, on a minimally rotated structural block. This provides a reference location for our paleomagnetic study to estimate relative vertical-axis rotation. A new $^{40}Ar/^{39}Ar$ age places the eruption of the JST at 12.114 ± 0.006 Ma. Anisotropy of magnetic susceptibility data, once corrected for local tilt and vertical axis rotation, yields a mean imbrication that trends 178°. The probable source of the JST is located in the Huntoon Valley/Queens Valley region. Eighteen paleomagnetic sites constrain mid-Miocene to recent vertical axis rotation within the region. All sites are discordant to the reference location with variable amounts of clockwise vertical axis rotation ranging from 25° to 104°. We hypothesize that a previously unrecognized early phase of deformation occurred that predates the deformation in the central Mina Deflection. These new data support the hypothesis that transtensional faulting associated with North American and Pacific plate interaction transferred deformation across the Mono Basin region that was partially accommodated by vertical axis rotation. By late Miocene, deformation had stepped east developing the Silver Peak-Lone Mountain detachment system followed by the structures that presently define the central Mina deflection. This study further demonstrates that deformation occurred east of the Sierra Nevada Mountains at the latitude of the Mono Basin in western-most Nevada, a region previously thought to be undeformed in terms of clockwise vertical axis rotation.

1. Introduction

The deformation between the North American and Pacific transform plate boundary is accommodated as brittle structures across a wide zone of the western margin of North America, from the San Andreas Fault east into the western Basin and Range Province (Figure 1; Bennett et al., 2003; Dixon et al., 1995, 2000, 2003; Kreemer et al., 2009; Malservisi et al., 2003; Miller et al., 2001; Oldow, 2003; Oldow et al., 2001; Thatcher et al., 1999). This zone accommodates about 25% of the distributed deformation between the Pacific and North American plates (Argus & Gordon, 1991; Bennett et al., 2003; Faulds & Henry, 2008; Foy et al., 2012; Minster & Jordan, 1987; Oldow, 2003). Present-day deformation is localized within the Eastern California Shear Zone to the south (Dokka & Travis, 1991, 1996) and the Walker Lane to the north (Locke et al., 1940; Stewart, 1980, 1981, 1984). These two systems are characterized by northwest trending faults and deformation that are indicative of transtensional deformation (Oldow, 1992a, 1992b, 2003). At the latitude of the southern Sierra Nevada north of the Garlock fault (Figure 1), displacement in the northern part of the Eastern California Shear Zone is concentrated within an ~250-km wide zone of right-lateral shear that is accommodated along three major strike-slip fault zones: (1) the Death Valley-Furnace Creek-Fish Lake Valley fault zone, (2) Hunter Mountain-Panamint Valley fault zone, and (3) the White Mountains-Owens Valley fault zones (Figure 2). The Sierra Nevada is a prominent geomorphic feature that rises to over 2,800 m. The range is bounded along its east flank by the Sierra Nevada frontal fault zone with the dextral Owens Valley fault located a few kilometers to the east. Arguably, the Owens Valley fault and the Sierra Nevada frontal fault define the western boundary of both the Eastern California Shear Zone and the Basin and Range Province, a region where northwest dextral shear has been superimposed on east-west extension (Frankel et al., 2011, and references therein). From south to north, the Eastern California Shear Zone narrows, and east of the
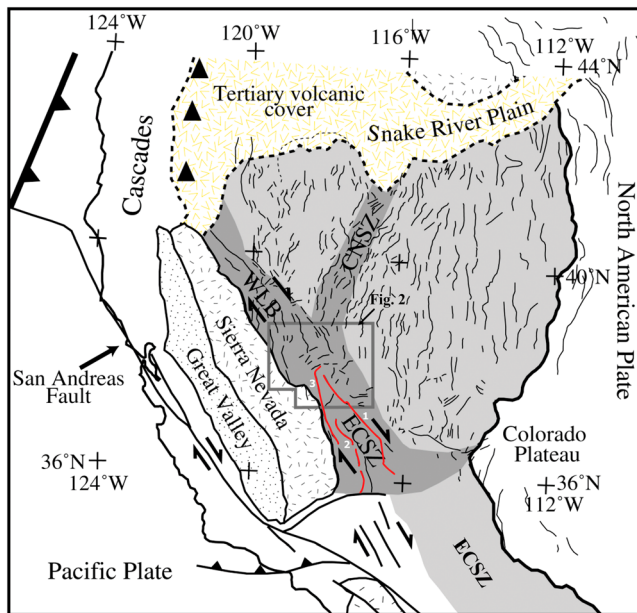
Figure 1. Simplified tectonic map of the central part of the western United States showing the major tectonic provinces, modern plate boundaries, and fault traces in the northern Basin and Range Province. Basin and Range province is in light gray; Walker Lane belt (WLB), Central Nevada seismic zone (CNSZ), and Eastern California shear zone (ECSZ) are in dark gray. Traces of Cenozoic faults in the northern Basin and Range are modified after Stewart (1988). Box denotes location of Figure 2. Numbers refer to major fault systems and these are highlighted red: (1) Death Valley-Furnace Creek-Fish Lake Valley, (2) Hunter Mountain-Panamint Valley, and (3) White Mountains-Owens Valley fault zones (map revised after Petronis et al., 2009).

central Sierra Nevada the northwest trending strike-slip fault systems abruptly swing eastward into an array of northeast-southwest to east-west striking faults, centered on the eastern Mono Basin, Adobe Hills, Candelaria Hills, and Excelsior Mountains, in the southern part of the central Walker Lane, known as the Mina deflection (Ryall & Priestly, 1975; Figure 2). These "z"-shaped curvilinear faults currently transfer much of the slip along the Furnace Creek-Fish Lake Valley and White Mountain-Owens Valley fault zones eastward to northwest trending transcurrent faults of the central Walker Lane and ultimately to the northern Walker Lane fault system and the Central Nevada Seismic Zone (Oldow, 1992a, 1992b, 2003; Oldow et al., 2001; Stewart, 1980; Wallace, 1984). Displacement transfer in this area initiated in the middle to late Miocene was facilitated by the development of the Silver Peak-Lone Mountain extensional complex (Oldow et al., 1994; Petronis et al., 2002, 2007), and evolved in the middle to late Pliocene into a more focused system of discrete east-northeast trending faults (Wesnousky, 2005).

In this contribution, we propose that Miocene deformation within the boundary zone between the Sierra Nevada block and the presently active central Mina Deflection was accommodated in the Mono Basin and south of the Excelsior Mountains prior to stepping east in the late Miocene into the present-day Walker Lane Belt and central Mina Deflection. To define deformation related to the initiation of displacement transfer between the Furnace Creek-Fish Lake Valley and White Mountain-Owens Valley fault zones and central Walker Lane fault systems, and thus test the hypothesis that a broad zone of deformation existed during the middle Miocene, we have collected paleomagnetic data from the Jack Springs Tuff (Gilbert et al., 1968; Stewart & Diamond, 1990). The Jack Springs Tuff is a regional ignimbrite likely sourced from a now buried vent located in the vicinity of the southern Huntoon Mountains-Queens Valley, NV region (Figure 2). This study assessed the magnitude, sense, and spatial variability of vertical axis rotations west of the central Mina Deflection in a region previously thought to be outside of the displacement transfer system (Oldow et al., 1994; Petronis et al., 2009; Wesnousky, 2005). The paleomagnetic results from the Jack Springs Tuff reveal that the regional extent of the area affected by clockwise vertical axis rotation is not confined to the central Mina Deflection in western Nevada. These data show that the area south and west of Huntoon Valley, Nevada into eastern California has experienced 25° to 104° of clockwise vertical axis rotation during a previously unrecognized phase of displacement transfer in this region.

2. Tectonic Setting

2.1. The Central Mina Deflection

Late Cenozoic faults, late Pleistocene to Holocene fault scarps, and modern seismicity indicate that the central Walker Lane Belt consists of arrays of variably oriented active faults characterized by northwest directed right-lateral shear and dip-slip fault motion (Faulds & Henry, 2008; Oldow, 1992a, 1992b, 2003; Stewart, 1988; Wesnousky, 2005). The northwest-southeast trending structural grain that characterizes the Walker Lane Belt is defined by an en echelon array of northwest trending strike-slip faults. When these faults enter the central Mina Deflection from the south-southeast, they swing east, defining a zone of predominantly east northeast trending oblique slip faults of late Pliocene and younger age, characterized by extensional and left-lateral fault motion. A few faults are mapped as continuous bends as they change in orientation, forming z-shaped releasing bends characterized by rhomboidal pull-apart basins that accommodate the strike-slip displacement (Ferranti & Oldow, 2005; Ferranti et al., 2009; Oldow, 1992a, 1992b; Figure 2). For example, southwest of Huntoon Valley, splays of the Excelsior
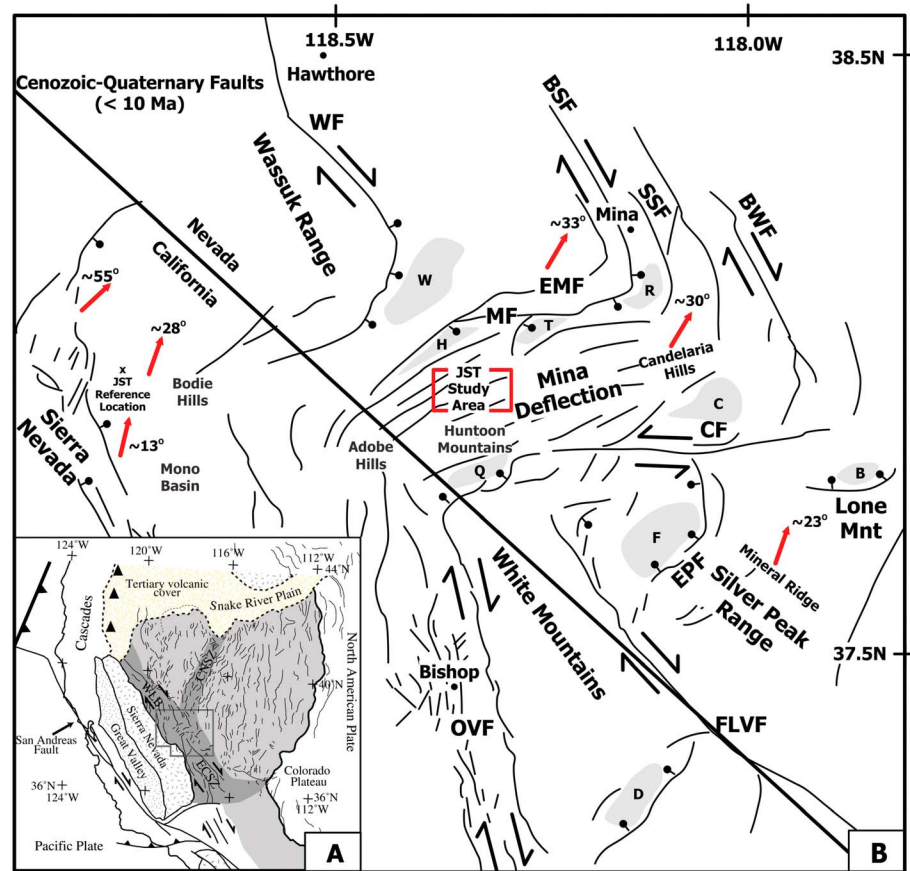
Figure 2. Simplified fault map of the Mina deflection and surrounding region. Diagram depicts late Cenozoic faults and locations of pull-apart structures in the Mina deflection area. *Pull-apart structures*: D, Deep Springs; F, northern Fish Lake Valley; H, Huntoon Valley; Q, Queen Valley; R, Rhodes Salt Marsh; B, southern Big Smokey Valley; T, Teels Salt Marsh; W, Whiskey Flat; C, Columbus Salt March area. *Late Cenozoic faults:* Wassuk fault, WF; Excelsior Mountain fault, EMF; Benton Springs fault, BSF; Soda Springs fault, SSF; Beetles Well fault, BWF; Coaldale fault, CF; Emigrant Peak fault, EPF; Death Valley-Furnace Creek-Fish Lake Valley fault zone, FLVF; White Mountains-Owens Valley fault zones, OVF. Hunter Mountain-Panamint Valley fault zone (not shown). The red arrows indicate areas that have experienced vertical axis rotation based on existing paleomagnetic data (e.g., Carlson et al., 2013; Petronis et al., 2002, 2007, 2009; Rood et al., 2011). Any deviation of the arrow from north indicates the approximate amount of vertical axis rotation (map modified after Petronis et al., 2009).

fault system swing south through the Adobe Hills, CA, and merge with faults that are part of the Owens Valley-White Mountain fault system (Figure 2). The Excelsior Mountains form part of the northern Mina Deflection, and are bounded to the south by the Marietta fault and related structures (Figure 2; Oldow, 1992a, 1992b; Wesnousky, 2005). The left-lateral Coaldale fault, located at the northern end of Fish Lake Valley, forms the southern boundary of the central Mina Deflection. The Coaldale fault zone currently transfers displacement east from the Owens Valley through the Queens Valley into the Big Smokey Valley and eventually northward into north-northwest trending structures of the central Walker Lane (Oldow, 1992a, 1992b; Reheis & Sawyer, 1997; Stockli, 1999; Lee et al., 2001, 2005; Tincher & Stockli, 2005; Figure 2). Previous paleomagnetic investigations in the Silver Peak Range (east to northeast area, Petronis et al., 2002; southwest area, Petronis et al., 2007) have shown that Miocene volcanic rocks in the upper plate of a regionally extensive, northwest dipping detachment system (the Silver Peak-Lone Mountain extensional complex), Miocene mafic intrusions in the lower plate, and late Cretaceous mafic dikes in the southwest Silver Peak Range have experienced net clockwise rotation of ~25° interpreted to be related to an "early" (middle to late Miocene to earliest Pliocene) phase of displacement transfer south of the central Mina Deflection (Petronis et al., 2009).

AGU
100
ADVANCING EARTH
AND SPACE SCIENCE

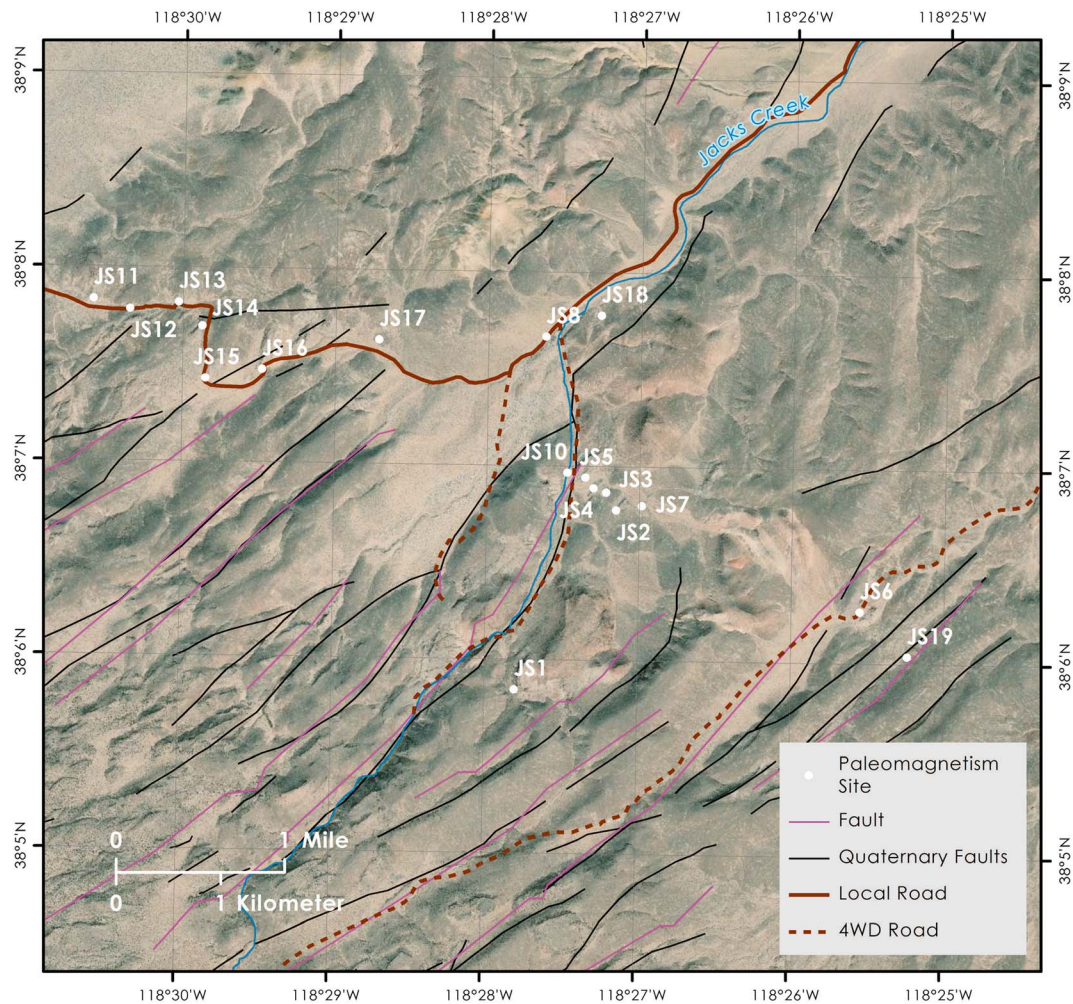**Geochemistry, Geophysics, Geosystems**

10.1029/2018GC007682

Figure 3. Simplified map of the sampling locations of the Jack Springs Tuff. Numbered solid circles are areas were paleomagnetic sampling sites were established (Tables 2 and 3). These locations are considered "structural blocks" (see text for discussion). JS1 is the informal type section of the Jack Springs Tuff where a near-complete ignimbrite section is preserved.

The west-central Walker Lane, west of the study area, has also experienced clockwise rotation, 11°–55° in discrete domains, since ~9.5 Ma (Carlson et al., 2013).

2.2. Southern Huntoon Valley Area

The Huntoon Valley is a northeast-southwest striking half-graben closed basin, bounded on the west and north by the Excelsior Mountains, NV, to the west-southwest by the Adobe Hills, CA, and to the east by the low hills south of Huntoon Valley and Teels Salt Marsh (Figure 3). There is little sign of recent fault activity other than local occurrences of oversteepening at the base of the range front and a number of well-developed triangular facets off the Excelsior Mountains on the northwest side of Huntoon Valley (Wesnousky, 2005). To the south and east, extending from Huntoon Valley across Teels Salt Marsh to HWY 360 is a region of low, fault-bounded hills where volcanic and sedimentary rocks are well exposed. The structural grain in this region is characterized by northeast-southwest striking oblique-slip faults of variable displacement that have fragmented the area into fault-bounded structural blocks. The present-day structural grain matches that within the central Mina Deflection. Prior to late Miocene faulting, the Jack Springs Tuff was emplaced across this region and has subsequently been fragmented and tilted into numerous fault-bounded discrete sections (Figure 4a). Compositionally, the Jack Springs Tuff is a sanidine and biotite crystal-rich ignimbrite (see below). Locally, the base of the section is exposed (Figure 4b) and the entire

Figure 4. Field photographs of the Jack Springs Tuff. (a) View to the northwest of several fragmented outcrops of the Jack Springs Tuff. Dotted red lines are concealed faults between the structural blocks. (b) Typical outcrop of the Jack Springs Tuff (1.7-m geologists for scale). Sampling site is located at the entrance to Jack Springs Canyon ~3 km from the base of the section depicted in (c). (c) Base of the Jack Springs Tuff at the informal type section showing the 1a and 1b layer of the ignimbrite. At this location, the tuff is exposed in its complete thickness of ~50 m and is capped by an andesite flow.

ignimbrite section is preserved at a location near the southern end of Jack Springs Canyon. More often, however, only part of the ignimbrite section is preserved (Figure 4c). We sampled paleomagnetic sites at 18 localities across this area, each from a separate structural block and at various levels within the ignimbrite. Our goals are to estimate relative vertical axis rotation between each block, to evaluate possible differential rotation in a region previously thought to be unrotated (Oldow et al., 1994; Petronis et al., 2009; Wesnousky, 2005), and to constrain the probable source region of the tuff.

3. Petrology of the Jack Springs Tuff

Representative polished thin sections of specimens were examined in transmitted and reflected light. There is slight variation in mineral assemblage and igneous texture between sites. All specimens contain abundant euhedral to subhedral phenocrysts of plagioclase and sanidine (Figure 5). Subhedral sanidine crystals are fragmented, some display magmatic exsolution textures, and several of the sanidine phenocrysts display zoning (Figure 5). Plagioclase crystals are euhedral and display little if any seritization. Euhedral, 3–7-mm biotite crystals are scattered throughout the matrix. Glomerocrysts are common and often contain a core of hornblende with biotite overgrowths. Estimated modal abundances classify these rocks as latite. In order of decreasing abundance, the typical mineral assemblages consist of plagioclase, sanidine, hornblende, biotite, titanomagnetite, ±quartz, and one sample (JS11_C2) contains xenocrysts of olivine. The glass matrix displays a distinctive eutaxic fabric defined by deformed fiamme and spinifex textures. Within the matrix, blocky Ti magnetites (<0.5–1 mm) and deformed biotite phenocrysts are common (Figure 5). Individual phenocrysts of sanidine and plagioclase occur as 2 mm and occasionally up to 5-mm crystals. Subhedral to euhedral phenocrysts of sanidine and plagioclase crystals are relatively unaltered with little if any
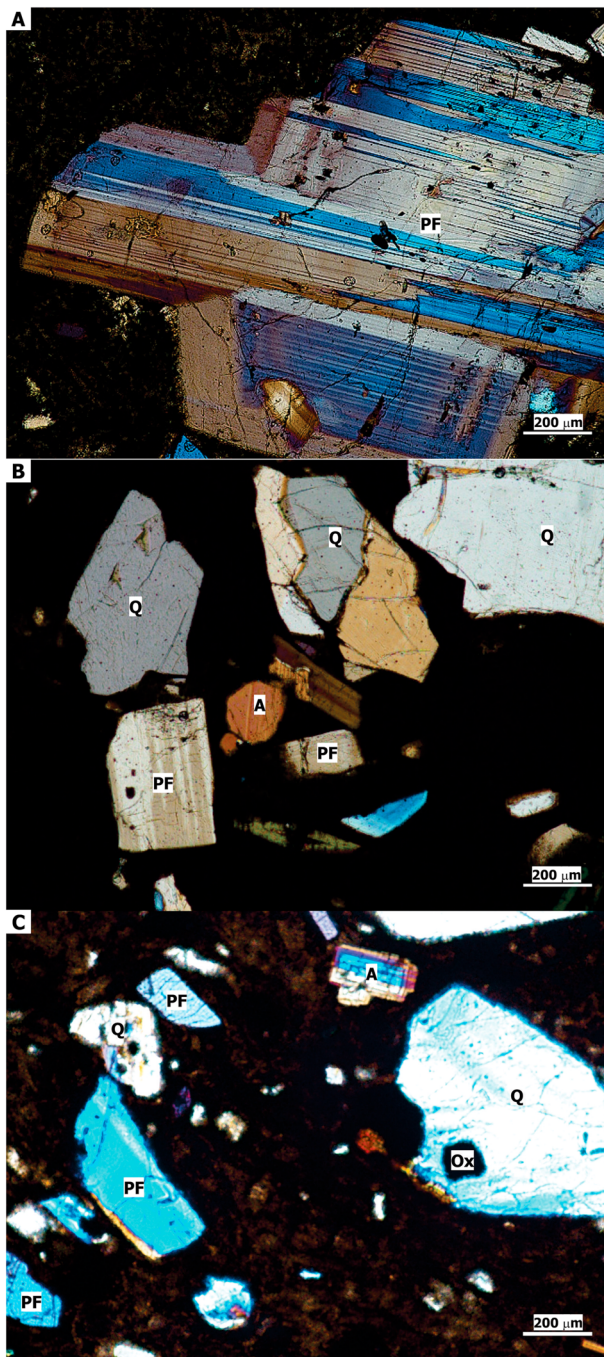
Figure 5. Photomicrographs of the Jack Springs Tuff. (a) Euhedral plagioclase feldspar phenocryst >2.0-mm length showing polysynthetic twinning in a very fine grained groundmass of feldspar microlites, Fe oxides, and glass. (b) Anhedral and fractured phenocrysts of quartz (0.2–0.3-mm diameter), euhedral lamellar twinned plagioclase feldspar (0.4 mm length), and euhedral augite (0.1-mm diameter) in a very fine grained groundmass. (c) Aligned euhedral lamellar twinned plagioclase feldspar and anhedral quartz phenocrysts measuring 0.1–0.4-mm length in a very fine grained glass-rich matrix. Augite is the hexagonal-shaped crystal in the top part of the photo.

seritization but are often highly fractured, typical of explosive pyroclastic rocks. Plagioclase phenocrysts are also found in glomerocrysts (~3–5 mm) with sanidine, hornblende, biotite overgrowths, and 1–2-mm oxides. Plagioclase phenocrysts in the glomerocrysts display simple twinning that is often more altered with a sieved texture. Sanidine phenocrysts typically show simple twins and are zoned, indicative of interrupted crystal growth. The inner rim of sanidine phenocrysts is relatively fresh with few if any titanomagnetite inclusions, while the outer rim of the crystals are rich in titanomagnetite and biotite inclusions. Hornblende phenocrysts occur in the glomerocrysts as well as aligning in the eutaxic fabric. In the glomerocrysts, subhedral hornblendes are ~2 mm, and are strongly overgrown by biotite. Within the glassy matrix, euhedral hornblende microphenocrysts are <1 mm and display two perfect cleavage planes. Euhedral biotite phenocrysts generally range from 1 to 2 mm with one large phenocryst reaching ~5 mm. Biotite phenocrysts often are present along the margins of feldspar phenocrysts and within glomerocrysts as well as within the glassy matrix. They are very fresh with little to no alteration, but larger phenocrysts of biotite do show some slight deformation and elongation along the eutaxic fabric (Figure 5).

4. Reference Location

Observed paleomagnetic declinations that deviate or are discordant from some expected value can provide rotation estimates that are in either an absolute or a relative framework. Absolute rotation determinations require a result that adequately samples the geomagnetic field over a sufficiently long time (e.g., a sequence of numerous basalt flows showing multiple polarity intervals) and that is compared with a sufficiently robust estimate of the time-averaged field direction, based on the field direction from the stable craton (Beck & Burr, 1979; Carlson et al., 2013; Gattacceca et al., 2007; Kamerling & Luyendyk, 1985; Luyendyk et al., 1985; Petronis et al., 2002, 2009; Simpson & Cox, 1977). Relative determinations, on the other hand, require sampling a single laterally extensive datum such as a regionally extensive ash flow tuff (e.g., Byrd et al., 1994; Petronis et al., 2014; Sussman et al., 2006; Wells & Hillhouse, 1989). Under ideal circumstances, where either a time-averaged geomagnetic field is exceptionally well sampled or a single datum consistently yields a high-precision result, estimates of absolute vertical-axis rotation typically have 95% confidence limits of about 4° to 10° and relative vertical-axis rotation estimates typically have confidence limits less than 5° (Petronis et al., 2009). Paleomagnetic investigations of ignimbrites reveal that individual cooling units typically yield an instantaneous record of the geomagnetic field (e.g., Byrd et al., 1994; Geissman et al., 1984; Reynolds, 1977; Wells & Hillhouse, 1989). Thus, combining results from a small number of discrete ash flow tuffs will not provide an adequate long-term average of the geomagnetic field. Our analysis of the data from the Jack Springs Tuff involved comparing results from the ignimbrite to data from four sites (John et al., 2012) at the edge of the Sierra Nevada microplate. This reference section lies within a region hypothesized by Carlson et al. (2013) to have experienced low rotation (<13°), as measured using widespread ignimbrites of the Stanislaus Group, which span the Sierra Nevada microplate and West-Central Walker Lane. The Bodie Hills clearly experienced Miocene deformation, so rotation estimates based on this reference section reflect a minimum rotation amount. To our knowledge, these

are the westernmost exposures of the Jack Springs Tuff identified (Figure 2). At all sites sampled and at the reference location, the Jack Springs Tuff consists of a single cooling unit emplaced during one explosive eruption (Figure 4). The ignimbrite serves as a single datum that has been subsequently fragmented into multiple structural blocks. Paleomagnetic data from the Jack Springs Tuff are compared to data from this reference section after the following corrections. The Jack Springs Tuff has been corrected for local tilt, based on one or more of the following: the orientation of eutaxitic fabrics, the orientations of oxidized flow tops, erosional breaks between units, or contacts with underlying or overlying sedimentary or volcaniclastic deposits. At the reference section in the Bodie Hills (John et al., 2012, 2015), the Jack Springs Tuff has a unique characteristic remanent magnetization that is well defined and of low dispersion. The characteristic remanent magnetization data from the reference section is $D = 353°$, $I = 43°$, $\alpha_{95} = 7.7°$, $n = 4$ sites (42 samples; Lindeman et al., 2013). Removing the 13° of vertical axis rotation (Carlson et al., 2013) provides an unrotated reference direction of $D = 340°$, $I = 43°$, $\alpha_{95} = 7.7°$. The well-defined characteristic remanent magnetization of the ignimbrite affords a relative estimate of vertical-axis rotation between separate structural blocks, where any deviation of the declination at individual sites compared to the reference section is interpreted as reflecting vertical axis rotation, provided that the inclination is near identical.

5. Analytical Methods

5.1. Field Methods

Eight to 10 drill core samples were collected at 18 sites, located on different fault blocks, using a modified Echo 280E gasoline powered drill with a nonmagnetic diamond tip drill bit. All samples were oriented using a magnetic and, when possible, a Sun compass. All core samples were cut into 2.2 × 2.5-cm right cylinder specimens, using a diamond tipped, nonmagnetic saw blade with up to three specimens per core sample obtained at New Mexico Highlands University's Rock Processing laboratory.

5.2. Rock Magnetism

To characterize the magnetic mineralogy, standard rock magnetic experiments were conducted with the goal of identifying the magnetic phases carrying the remanence, and the overall ability of these rocks to faithfully record an ambient field. Equipment used include an AGICO JR6A dual-speed spinner magnetometer, home-built and ASC Scientific (Model IM-10-30) static impulse magnets capable of 1 to 3-T peak fields, Lake Shore Cryotronics MicroMag 2900/3900 Vibrating Sample Magnetometer, and a Quantum Design 7-T magnetic property measurement system. All susceptibility experiments were measured with an AGICO MFK1-A kappabridge susceptibility meter with a CS4 high-temperature attachment at the New Mexico Highlands University Paleomagnetic-Rock Magnetic laboratory. Hysteresis measurements were conducted on a Lake Shore Cryotronics MicroMag 2900/3900 Vibrating Sample Magnetometer at the University of Texas-Dallas paleomagnetism laboratory. Hysteresis experiments involved vibrating the sample within a 3.0 T applied field at 83 Hz next to a set of pickup coils. The vibrating sample creates a time-varying magnetic flux in the coils, generating a current that is proportional to the sample's magnetization. In order to characterize the magnetic mineralogy, and complement hysteresis experiments, we conducted room temperature saturation isothermal remanent magnetization SIRM, low-temperature SIRM (LTSIRM), field cooled (FC), and zero field cooled (ZFC) experiments with a Quantum Design 7-T magnetic property measurement system system. The magnetic property measurement system experiments are used primarily for magnetic mineral identification based on low-temperature crystallographic transitions (e.g., the Verwey transition; Verwey, 1939), and for characterizing particle size distributions. To evaluate the stability of an induced remanence on cooling and warming we performed (1) low-temperature (LT) cycling on cooling from 300to 10 K of a room temperature (RT) saturation isothermal remanence and (2) LT saturation isothermal remanence (LTSIRM) cycling on warming from 10 to 300 K. For the first experiment, the specimen is given a saturation magnetization in a 2.5-T DC field while at 300 K. Magnetic remanence measurements are performed as the specimen is cooled to 10 K. For the second part of this experiment, while at 10 K a second 2.5-T saturation magnetization (LTSIRM) is imparted and the remanence is measured on warming back to room 300 K. The next part of the experiment involves the sample being cooled in a sustained DC field of 2.5 T to 10 K. The field is then switched off at 10 K and the magnetic remanence is measured as the specimen warms back up to room temperature (FC remanence). The

specimen is then subsequently cooled in a null magnetic field (ZFC) to 10 K, where a LTSIRM is imparted and the remanence is measured again on warming back to room temperature (ZFC remanence). The ratio of the δFC/δZFC (Moskowitz et al., 1993) and the ratio of M1/M5 (Smirnov, 2009) provides an estimate of the magnetic domain state. The magnetic domain state of the grain is single domain when the δFC/δZFC ratio is greater than 1 and the M1/M5 ratio is between 1 and ~1.3. Values less than or equal to 1 are indicative of all other magnetic domain sizes (e.g., multidomain). It is important to note that the δFC/δZFC and M1/M5 ratios are a best estimate of magnetic domain state but the results are often not 100% conclusive. The magnetic susceptibility of titanomagnetite strongly depends on the composition of the Fe-Ti oxides with the bulk susceptibility being a function of Ti composition and applied field amplitude (Jackson et al., 1998; de Wall, 2000; Hrouda et al., 2002). The percentage of field dependence (χHd) is (χ300 A/m − χ30 A/m) χ300 A/m and expressed as a percentage. Curie point estimates were conducted using an AGICO MFK1-A kappabridge susceptibility meter with a CS4 high-temperature attachment. These experiments are used to establish the dominant magnetic mineral phase(s) present in the sample and to define the composition of the titanomagnetite phase(s).

5.3. The ^{40}Ar/^{39}Ar Analytical Methods

Sanidine phenocrysts were collected from crushed samples by magnetic and hand-picking methods. The mineral separates and monitors (Fish Canyon tuff sanidine, 28.201 Ma; Kuiper et al., 2008) were loaded into aluminum discs and irradiated for 16 hr at the USGS TRIGA reactor in Denver, CO. The samples were step-heated with a Photon Machines Diode laser and analyzed with a Thermo Argus VI mass spectrometer at the New Mexico Geochronology Research Laboratory. Abbreviated analytical methods for the dated samples and the argon isotopic data are given in Appendix A, and the details of the overall operational methods of the New Mexico Geochronology Research Laboratory are provided on their website at https://geoinfo.nmt.edu/labs/argon/methods/home.html. The age results are summarized in Table 1.

5.4. Anisotropy of Magnetic Susceptibility Methods

Anisotropy of magnetic susceptibility (AMS) measurements of a rock specimen yield an ellipsoid of magnetic susceptibility (K) defined by the length and orientation of its three principal axes, $K_1 \geq K_2 \geq K_3$, which are the three eigenvectors of the susceptibility tensor (Tarling & Hrouda, 1993). The long axis of the magnetic susceptibility ellipsoid, K_1, gives the magnetic lineation, while the short axis, K_3, defines the normal to the magnetic foliation plane (K_1-K_2). The bulk magnetic susceptibility (K_m) is the arithmetic mean of the principal axes K_1, K_2, and K_3 (see Jelínek 1981; Tarling & Hrouda, 1993). We measured the AMS of 398 specimens prepared from samples collected at 18 sites distributed throughout the study area. The AMS measurements were performed on an AGICO MFK1-A multifunction kappabridge operating at low alternating field of 200 A/m at 976 Hz at the New Mexico Highlands University Paleomagnetic-Rock Magnetic laboratory. The results are summarized in Table 2 and the susceptibility parameters, transport direction, and anisotropy of magnetic susceptibility data from each site are contained in Appendix B.

5.5. Paleomagnetic Methods

At most paleomagnetic localities sampled, the orientation of the deposits, and thus stratal dip estimates, were defined principally using the orientation of eutaxitic fabrics, but also, when possible, the orientations of oxidized flow tops, erosional breaks between units, and contacts with underlying or overlying sedimentary or volcaniclastic deposits. Implicit in any correction based on eutaxitic fabrics is the assumption that pumice compaction defines a paleohorizontal datum, at the time of remanence acquisition. Although this is commonly the case, significant differences between the paleohorizontal and a eutaxitic fabric can occur if the deposit was emplaced onto irregular topography or confined to a high-relief channel. In addition, post-emplacement flow (rheomorphism) can result in eutaxitic fabrics of variable orientation (Tarling & Hrouda, 1993). At all locations sampled, we did not see evidence of rheomorphism and sites were collected from areas where the ignimbrite maintained a visibly uniform thickness over as much distance as possible to avoid potential paleochannel margins. It was assumed that the compaction fabrics developed parallel to the underlying topography and that slopes were close to horizontal and thus the current orientation of the deposits is a reflection of postemplacement local tectonic tilt. Although considerable effort was made to accurately define the orientation of each deposit (typically 5 to 15 strike and dip measurements of eutaxitic fabrics at each

Table 1
Summary of $^{40}Ar/^{39}Ar$ Results

Sample	Lab #	Mineral	Age Analysis	Step/Analysis	Age (Ma)	±2 Sigma (Ma)	MSWD
JS-1	65098	Sanidine	Laser fusion	14	12.114	0.006	5.36

Note. Sample name (see Figure 3 for location); lab #, laboratory identification number; mineral, mineral analyzed; age analysis, laser fusion method; step/analysis, number of sanidine crystals measured; age (Ma); calculated weighted mean age; ±2 sigma (Ma), age estimate error; MSWD, mean square weighted deviation.

locality), sites where dips of inferred paleohorizontal indicators are high, may have relatively large errors associated with the corrected data. Chan (1988) evaluated how apparent rotations can arise in declination data if an inappropriate tilt correction is applied, and specifically emphasized that the magnitude of apparent rotation may increase with the magnitude of the tilt correction. The typical dip values measured in the Jack Springs Tuff averaged 24.1° ± 11.0° and ranged from 6° to 44° (Table 3). The outcrop pattern of the ignimbrite is admittedly not always ideal because of Miocene faulting and tilting of the ignimbrite sheet (Figure 4a). The orientation of the ignimbrite at some localities was difficult to determine because exposures are discontinuous, well-exposed bases of the sequences and contacts with underlying sedimentary-stratified rocks are uncommon, and/or compaction foliations are sometimes poorly defined. Although we attempted to avoid these potential problems, in some cases they are unavoidable, and occasional poorly defined paleohorizontal information likely contributes to dispersion (specifically, sites exhibiting inclination deviation) of the paleomagnetic data.

Remanent magnetizations of all samples were measured using an AGICO JR6A dual-speed spinner magnetometer at the New Mexico Highlands University Paleomagnetic-Rock Magnetic laboratory. Specimens were progressively alternating field (AF) demagnetized, typically in 10 to 25 steps, to a maximum field of 120 mT using a ASC Scientific D-TECH 2000 AF-demagnetizer. Samples with high coercivity were treated with thermal demagnetization (TH) up to a maximum of 630 °C, yet with most samples being fully demagnetized by 580 °C. Thermal demagnetization experiments on replicate specimens, to compare with AF behavior, were conducted with an ASC Scientific TD48 thermal demagnetizer. Principal component analysis (Kirshvinck, 1980) was used to determine the best fit line through selected demagnetization data points for each sample using Remasoft 3.0 (Chadima & Hrouda, 2006; Figure 6 and Table 3). For most samples, a single best fit line could be fit to the demagnetization data points. Best fit magnetization vectors involved 5 to 18 data points, but as few as 3 to as many as 25 were used, and for less than 10% of the samples it was necessary to anchor them to the origin. Magnetization vectors with maximum angular deviation values greater than 5° were not included in site mean calculations.

6. Results

6.1. Rock Magnetic Experiment Results

As described, rock magnetic experiments were conducted to determine the magnetic mineralogy and domain state of the principle magnetization carriers in the Jack Springs Tuff. These included Curie point estimates, magnetic susceptibility as a function of field amplitude from 2 to 700 A/m, magnetic property measurement system data, and hysteresis experiments. As indicated in the following subsections, the rock magnetic data indicate that the dominant magnetic mineral phase is a cubic Fe-Ti oxide of a restricted magnetic grain size, primarily pseudosingle-domain titanomagnetite and coarse-grained maghemite.

6.2. Low-Field Susceptibility Versus Temperature

Five samples from different parts of the ignimbrite yield a narrow spectrum of results that show irreversible curves with two or more Curie point estimates. During heating, the samples show an increase in magnetic susceptibility followed by a decrease (a "bump") in susceptibility over the interval from 300 °C to 350 °C. During the cooling stage, the bump is not observed, which can be interpreted to reflect the homogenization of exsolved Fe-Ti oxide into a single titanomagnetite phase during the heating experiment, likely coarse-grained maghemite or an Fe sulfide phase (Figure 7; Özdemir & O'Reilly, 1981, 1982). On further heating up to ~550 °C to 580 °C, all samples yield a rapid drop in susceptibility indicative of a Curie point for near-stoichiometric magnetite. Curie point estimates indicate that the titanium concentration of the high-

Table 2
Anisotropy of Magnetic Susceptibility Data From the Jack Springs Tuff

Site	No	N	Km	In situ K1	K2	K3	K1-K2	STRIKE/DIP	Tilt Corrected K1	K2	K3	K1-K2	Vertical Axis
			(10–3 SI)										Rotation
JS1	17	17	17.0	152/15	245/12	012/71	102,19 S	129, 18 NE	146/21	248/28	024/54	114, 36 S	56
JS2	25	25	17.6	110/00	200/02	015/88	105, 02 S	033, 28 SE	288/27	020/04	131/48	221, 42 W	30
JS3	23	23	17.3	006/11	274/10	143/75	223, 15 N	010, 06 NW	005/11	274/04	164/79	254, 11 N	52
JS4	21	21	13.4	245/21	338/10	092/67	182, 23 W	010, 06 NW	246/16	337/07	089/73	179, 17 W	68
JS5	23	23	15.0	115/25	212/15	330/60	060, 30 S	129, 14 NE	109/21	211/29	348/53	078, 37 S	25
JS6	23	23	16.6	177/09	269/14	056/74	146, 16 W	163, 15 SW	174/12	271/28	064/59	154, 31 W	58
JS7	21	21	16.0	029/13	124/19	266/67	356, 23 E	033, 20 SE	039/14	304/06	208/76	298, 14 N	59
JS8	23	23	18.2	242/06	333/08	115/80	205, 10 W	n/a	242/06	333/08	115/80	205, 10 W	64
JS10	27	27	17.3	119/27	218/17	336/57	066, 33 S	052, 44 SE	301/14	210/03	129/67	219, 23 W	104
JS11	24	24	13.1	092/09	186/20	339/68	069, 22 S	044, 18 SE	273/05	183/08	031/81	121, 21 E	60
JS12	23	23	12.7	023/07	124/59	289/31	019, 59 E	028, 39 SE	029/09	121/20	276/69	006, 21 E	21
JS13	24	24	13.1	061/17	178/55	321/30	051, 60 S	041, 36 SE	067/03	159/26	332/65	062, 25 S	52
JS14	21	21	13.5	054/06	147/25	311/64	041, 26 E	028, 37 SE	233/10	324/08	092/77	182, 13 W	74
JS15	25	25	15.1	161/29	067/03	334/61	064, 29 S	046, 27 SE	158/04	246/07	041/81	131, 09 S	77
JS16	25	25	12.5	202/28	109/06	008/61	098, 29 S	308, 25 SW	204/04	113/13	311/76	041, 14 E	33
JS17	19	19	13.2	274/70	169/05	077/19	167, 71 W	238, 30 NW	191/66	351/23	084/07	174, 83 W	89
JS18	18	18	20.5	066/09	336/03	226/81	316, 09 E	035, 26 SE	247/05	340/25	146/64	236, 26 N	91
JS19	16	16	16.3	305/45	202/13	100/42	190, 48 W	340, 20 NE	005/50	180/40	271/03	002, 87 E	65

Note. Anisotropy of magnetic susceptibility data. N_o = number of accepted specimens; N = number of specimens analyzed at each site; K_m = mean bulk susceptibility; K_1, K_2, and K_3 = trend and plunge (in degrees) of maximum, intermediate, and minimum susceptibility axes; K_1-K_2 = strike and dip of the magnetic foliation plane; strike/dip of the ignimbrite based on eutaxitic fabric or contact with underlying deposits; tilt corrected, trend and plunge of K_1, K_2, and K_3 axes and K_1-K_2 plane following correction for the strike/dip of the deposit; vertical axis rotation, trend and plunge of K_1, K_2, and K_3 axes and K_1-K_2 plane following correction for paleomagnetic derived vertical axis rotation with respect to the reference area (Beck, 1980; Demarest, 1983); L = ratio of K_1/K_2; F = ratio of K_2/K_3; P_j = corrected anisotropy degree; T = shape parameter; UTM coordinates datum WGS 84.

temperature titanomagnetite phase ranges from 0.004 to 0.019 (Akimoto, 1962), and this phase carries a thermoremanent magnetization (Table 4). In summary, the thermomagnetic experiments indicate that the dominant magnetic mineral in all of the samples is a ferromagnetic phase, most likely low-Ti titanomagnetite and a low-temperature coarse-grained titanomaghemite phase, as we did not see any Fe-sulfide phases in thin section.

6.3. Magnetic Susceptibility as a Function of Field Amplitude

The results from these experiments (Figure 8) indicate little field dependence in susceptibility (0.07% to 1.59% with a mean of 0.38%; $n = 8$) and that the Ti content of the titanomagnetite is low, consistent with the Curie point estimates (Akimoto, 1962).

6.4. Magnetic Property Measurement System

RT and LT remanence/temperature curves are presented for three samples (Figure 9a). In general, the three samples on cooling from 300 K show little to no decrease or increase in remanence indicating that the magnetic moments of the materials do not have a dependence on temperature and that the zero field in the chamber is very low. A lack of field dependence on cooling is typical of ferromagnetic ordering behavior (Dunlop & Özdemir, 1997). Following application of the low-temperature SIRM at 10 K, the large initial remanence on the warming curves is the LTSIRM and does not reflect a paramagnetic component. On further warming, the samples all show a rapid loss of remanence from 10 to ~160 K with a near-linear decrease in remanence from 160 to 300 K. We do not see any diagnostic crystallographic phase transitions, and we attribute the lack of a pronounced Verwey transition at ~120 K to the presence of impurities (Ti), which suppresses the transition (e.g., Özdemir et al., 1993; Özdemir & Dunlop, 1997).

The FC-ZFC low-temperature experiments reveal near-identical behavior between the three samples analyzed with a sharp loss in remanence over the temperature interval of 10 to 150 K followed by a near-

Table 2 *(continued)*

Site	K1	Rotation Corrected			L	F	Pj	T	Shape	UTM WGS 84	
		K2	K3	K1-K2						Northing	Easting
JS1	090/21	192/28	328/54	058, 36 S	1.000	1.011	1.012	0.959	O	4217635	371691
JS2	258/27	350/04	101/48	191, 42 W	1.002	1.012	1.015	0.729	O	4219338	372668
JS3	313/11	222/04	112/79	202, 11 W	1.003	1.013	1.022	0.672	O	4219511	372572
JS4	178/16	269/07	021/73	111, 17 S	1.002	1.017	1.021	0.776	O	4219551	372451
JS5	084/21	186/29	323/53	053, 37 S	1.003	1.015	1.019	0.651	O	4219653	372371
JS6	116/12	213/28	006/59	096, 31 S	1.002	1.015	1.019	0.741	O	4218367	374990
JS7	340/14	245/06	149/76	239, 14 N	1.003	1.014	1.018	0.640	O	4219381	372913
JS8	178/06	269/08	051/80	141, 10 W	1.002	1.018	1.022	0.758	O	4221000	372000
JS10	197/14	097/03	025/67	115, 23 S	1.003	1.014	1.018	0.630	O	4219700	372200
JS11	213/05	123/08	331/81	061, 09 S	1.001	1.018	1.021	0.912	O	4221377	367677
JS12	008/09	100/20	255/69	345, 21 E	1.004	1.013	1.018	0.541	O	4221276	368026
JS13	015/26	107/26	280/65	010, 25 E	1.000	1.012	1.014	0.961	O	4221339	368492
JS14	159/10	250/08	018/77	108, 13 S	1.002	1.013	1.016	0.788	O	4221108	368716
JS15	081/04	169/07	324/81	054, 09 S	1.000	1.019	1.022	0.974	O	4220609	368739
JS16	171/04	080/13	278/76	008, 14 E	1.004	1.013	1.018	0.515	O	4220692	369284
JS17	102/66	262/23	355/07	085, 83 S	1.002	1.010	1.014	0.612	O	4220975	370405
JS18	156/05	249/25	055/64	145, 26 W	1.005	1.012	1.018	0.366	O	4221200	372529
JS19	300/50	115/40	206/03	296, 87 N	1.004	1.013	1.018	0.481	O	4217934	375441

linear loss of remanence to 300 K. We see no evidence of a diagnostic crystallographic phase transition (Verwey, 1939; Verwey et al., 1947). The FC remanence is slightly higher than the ZFC remanence indicative of single-domain titanomagnetite and the two curves converge at ~50 K (JS1, JS8) and ~150 K (JS14), respectively (Figure 9b). The ratio of δFC/δZFC and M1/M5 are all greater than 1.0 and between 1.0 and 1.3, respectively, consistent with a single-domain grain size (Moskowitz et al., 1993; Smirnov, 2009). The lack of strong field dependence above 100 K for these samples on warming is diagnostic of ferromagnetic ordering behavior of a single domain to pseudosingle-domain magnetic grain size. An alternative, albeit speculative interpretation of these data based on the results of the other rock and paleomagnetic data, is that the samples contain a fraction of nanoparticles that are stable single-domain grain sizes at low temperature and become superparamagnetic (SP) as it unblocks on warming, with the shape of the curve showing the distribution of unblocking temperatures (particle volumes; Jackson & Swanson-Hysell, 2012) or the presence of titanohematite (Sprain et al., 2016).

6.5. Vibrating Sample Magnetometer-Hysteresis Results

The ratio of saturation remanence/saturation magnetization (Mrs/Ms) and the ratio of remanent coercive force ordinary coercive force (Hcr/Hc) are commonly used as indicators of domain states and, indirectly, magnetic grain size (e.g., Day et al., 1977; Dunlop & Özdemir, 1997; Parry, 1982). For magnetite, high values of Mr/Ms (>0.5) indicate (~0.05–0.08 μm) single-domain grains, and low values (<0.05) are characteristic of (~10–20 μm) multidomain (MD) grains. The intermediate regions are referred to as pseudosingle-domain grains with values from 0.5 to 0.05. Hcr/Hc is a less dependable parameter, but normally single-domain grains have a value less than 2, and MD grains should have values >4 (Day et al., 1977; Dunlop, 2002). Hysteresis loops for the two samples, one from the base and one toward the top of the ignimbrite, show steep acquisition reaching saturation by 0.150 to 0.250 T consistent with a pseudosingle-domain grain size (Figures 10a and 10b). We see no evidence of "wasp-waisted" shaped loops indicative of a mixture of magnetic grain sizes. The grains are magnetically hard, have high coercivities and remanence, and plot within the pseudosingle-domain field on a Day plot (Figure 10c). In summary, the rock magnetic data and demagnetization behavior indicate that the dominant magnetic phase is cubic Fe-Ti oxide of a restricted magnetic grain size between pseudosingle to single-domain titanomagnetite.

Table 3
Paleomagnetic Data From the Jack Springs Tuff, Western Nevada

SITE	N/no	R	k	α95	In Situ DEC	In Situ INC	VGP P_Lat	VGP P_Long	Strike/dip	Corrected DEC	Corrected INC	VGP P_Lat	VGP P_Long	R	Delta R	F	Delta F	UTM (WGS84) Northing	Easting
JS1	7/8	6.9	105.2	5.9	034.7	50.0	60.6	335.7	129, 18 NE	035.7	32.0	52.4	355.8	55.9	8.6	10.7	6.6	4217635	371691
JS2	6/8	5.9	239.2	4.3	033.4	42.3	58.6	347.8	033, 28 SE	010.2	36.6	69.9	327.0	30.4	8.2	6.1	6.4	4219338	372668
JS3	4/8	3.9	158.4	7.3	037.6	43.4	55.9	342.6	010, 06 NW	032.2	45.9	60.9	344.6	52.4	11.3	−3.2	8.4	4219511	372572
JS4	6/8	5.9	170.3	5.1	050.5	25.9	39.3	346.6	010, 06 NW	048.0	29.7	42.4	346.3	68.2	8.0	13.0	8.1	4219551	372451
JS5	6/8	5.9	647.6	2.6	010.6	33.5	68.3	394.0	129, 14 NE	004.6	45.5	77.9	318.1	24.8	8.2	−2.8	8.1	4219653	372371
JS6	8/8	7.9	462.7	2.6	044.2	30.7	45.8	348.6	163, 15 SW	038.2	43.5	55.4	342.4	58.4	8.2	−0.8	8.9	4218367	374990
JS7	5/8	4.9	1522.4	2.0	018.1	46.2	71.5	001.5	033, 20 SE	039.0	48.0	56.5	335.3	59.2	8.4	−5.3	9.7	4219381	372913
JS8	7/8	6.9	189.2	4.4	043.4	46.1	52.4	335.1	n/a	043.4	46.1	52.3	335.5	63.6	9.4	−3.4	11.0	4221000	372000
JS10	8/8	7.9	143.9	4.6	008.7	34.4	69.4	037.9	052, 44 SE	083.9	36.2	17.0	319.3	104.1	8.5	6.5	11.8	4219700	372200
JS11	8/8	7.9	433.1	2.7	025.9	36.2	61.3	003.3	044, 18 SE	039.8	39.7	52.6	345.1	60.0	8.0	3.0	12.2	4221377	367677
JS12	7/8	6.9	84.5	6.6	347.7	30.0	65.5	091.4	028, 39 SE	359.0	40.0	74.6	295.0	21.2	10.2	2.7	13.8	4221276	368026
JS13	5/8	4.8	32.5	13.6	008.8	27.1	65.1	041.3	041, 36 SE	032.2	40.3	58.5	351.7	52.4	16.2	2.4	17.4	4221339	368492
JS14	5/8	4.9	511.7	3.4	007.0	51.1	81.5	017.0	028, 37 SE	054.0	49.2	45.2	325.5	74.2	9.2	−6.5	14.7	4221108	368716
JS15	8/8	7.9	102.0	5.5	023.8	48.0	68.3	349.3	046, 27 SE	056.3	51.0	44.1	322.4	76.5	10.8	−8.3	15.8	4220609	368739
JS16	7/8	6.8	26.9	11.9	020.5	27.3	60.2	018.8	308, 25 SW	013.0	57.7	79.8	333.8	33.2	20.1	−15.0	18.6	4220692	369284
JS17	4/8	3.8	31.7	16.6	080.5	17.3	12.9	330.8	238, 30 NW	068.8	26.1	25.0	333.8	89.0	16.2	16.6	21.4	4220975	370405
JS18	6/7	5.9	756.3	2.4	009.2	67.2	76.3	267.8	035, 26 SE	070.9	64.5	38.8	298.6	91.1	10.1	−21.8	17.7	4221200	372529
JS19	7/8	6.9	53.1	8.4	042.5	26.1	45.3	353.1	340, 20 NE	045.2	08.1	36.6	359.6	65.4	15.5	34.6	19.6	4217934	375441

Note. Site, site name; N/N_o, number of specimen means used in site mean to total number of specimens means at the section; Dec/Inc, site declination and inclination; R, resultant vector length; k, best estimate of (Fisher) precision parameter; α95, 95% confidence interval of the estimated site mean direction assuming a circular distribution; VGP Lat/Long, latitude and longitude of the virtual geomagnetic pole; strike/dip = strike and dip of unit based on eutaxitic fabric or contact with underlying deposits; Dec/Inc corrected = stratigraphicaly corrected declination and inclination; rotation (R) and flattening (F) and associated error estimates (±R, ±F) after Beck (1980) and Demarest (1983) with respect to the Bodie Hills ignimbrite section. See text for discussion; UTM coordinates datum WGS 84.

6.6. The $^{40}Ar/^{39}Ar$ Analytical Results

Fourteen single crystals of sanidine from JS-1 were analyzed; all 14 were used to calculate a weighted mean age of 12.114 ± 0.006 Ma (Table 1 and Appendix A). The radiogenic yields of these samples range from 93.4% to 99.5% and the K/Ca ratios are very uniform ranging from 27.0 to 35.6. The weighted mean age of all 14 of the analyzed crystals of sanidine from JS-1 provide precise and what we interpret as accurate eruption age. The results from the new $^{40}Ar/^{39}Ar$ age determination further refine previously published K-Ar (Kleinhampl et al., 1975) and $^{40}Ar/^{39}Ar$ ages (John et al., 2012).

6.7. Anisotropy of Magnetic Susceptibility Results

Table 2 summarizes all magnetic susceptibility data and key magnetic parameters and individual susceptibility plots are shown in Appendix B. K_m intensities (in the SI system) are high, and yield values from 12.5×10^{-3} SI to 20.5×10^{-3} SI with a mean of $15.5 \times 10^{-3} \pm 2.3 \times 10^{-3}$ SI. The AMS fabric results yield susceptibility ellipsoid shapes that are all strongly oblate (average $T = 0.7 \pm 0.17$; Table 2). The corrected degree of anisotropy (P_j; Jelínek 1981) varies between 1.022 and 1.014, and averages 1.018 ± 0.003, indicating a weak (~2%) degree of anisotropy. The magnetic lineation (L) and foliation (F) averaged 1.002 ± 0.002 and 1.014 ± 0.003, respectively. There is no correlation between the corrected degree of anisotropy (P_j) and mean susceptibility (K_m) and no correlation between the shape parameter (T) and K_m (Appendix B). The bedding tilt corrected and vertical axis rotation corrected magnetic foliation planes yield a mean imbrication directed to the south-southeast with an average imbrication trend of 178° (Appendix B).

6.8. General Demagnetization Behavior

For most samples the overall progressive AF demagnetization response, defined over a broad range of peak fields, is characterized by a nearly linear trend to the origin. Most samples yielded a single-component normal polarity magnetization that decayed linearly to the origin with less than 10% of the NRM remaining after treatment in 80- to 120-mT applied fields (Figure 6). A few samples contained additional low-coercivity viscous remanent magnetization components that were readily randomized by 20 mT (Figure 6). The Jack Springs Tuff yields median destructive fields between 20 and 60 mT, and this behavior is characteristic of multidomain (MD), pseudosingle-domain, to single-domain titanomagnetite phase; these are the dominant ferromagnetic grains that carry the remanence and AMS fabric. The structurally corrected (based on one of the following or more, the orientation of eutaxitic fabrics, the orientations of oxidized flow tops, erosional breaks between units, or contacts with underlying or overlying sedimentary or volcaniclastic deposits) results for the 18 sites yield east-northeast declinations and moderate, positive inclinations. We compared the individual site
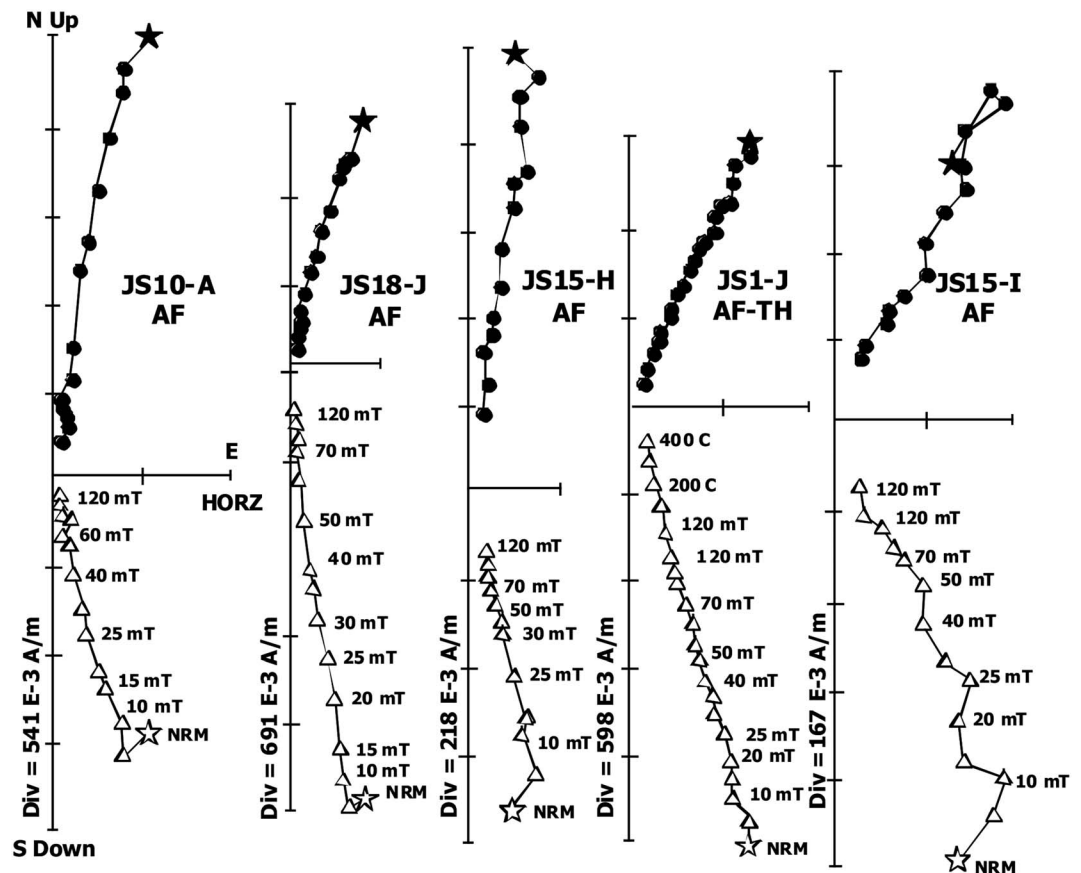
Figure 6. Orthogonal demagnetization diagrams representing the typical AF and TH demagnetization behavior (Zijderveld, 1967). Solid (open) symbols represent the projection onto the horizontal (vertical) plane. The demagnetization steps are given in mT and temperature (*T*, °C). Magnetization (in A/m) is shown along one axis for each sample; each division equals indicated intensity. A few samples contained additional low-coercivity viscous remanent magnetization (VRM) components that were readily randomized by 20 mT.

means to the paleomagnetic data from the unrotated reference direction of $D = 340°$, $I = 43°$, $\alpha_{95} = 7.7°$ (Lindeman et al., 2013), and our results indicate a range of discordant data, interpreted to reflect clockwise vertical axis rotation with rotation (*R*) estimates from $R \pm \Delta R = 24.8° \pm 11.2°$ to $104.1° \pm 10.8°$ (Table 3).

7. Discussion

The western Great Basin, parts of which have been considerably modified by the well-recognized system of right-lateral faults defining the Walker Lane, accommodated a significant amount of cumulative deformation via crustal block rotation in response to different phases of Miocene deformation. Rigid body rotations about a vertical axis are not always straightforward to identify, quantify, or explain. Yet numerous paleomagnetic studies have documented variable degrees (or lack thereof) of vertical axis rotation associated with strike-slip faulting and extension in the Cordillera and the Great Basin (e.g., Carlson et al., 2013; Cashman & Fontaine, 2000; Faulds & Varga, 1998; Gillett & Vanalstine, 1982; Hudson & Geissman, 1985; Hudson et al., 1994, 1998; Janecke et al., 1991; Petronis et al., 2002, 2007, 2009, 2014; Ron et al., 1984; Rood et al., 2011). The active transtensional fault system in the central Mina Deflection area links northwest trending dextral faults of the Furnace Creek-Owens Valley-Fish Lake Valley fault system to structures of similar orientation in the central Walker Lane by transferring displacement in an extensional right step along a relatively narrow system of roughly east-west striking left-oblique slip faults (Oldow et al., 1994; Wesnousky, 2005). This general area is well documented by geologic, seismic, and geodetic
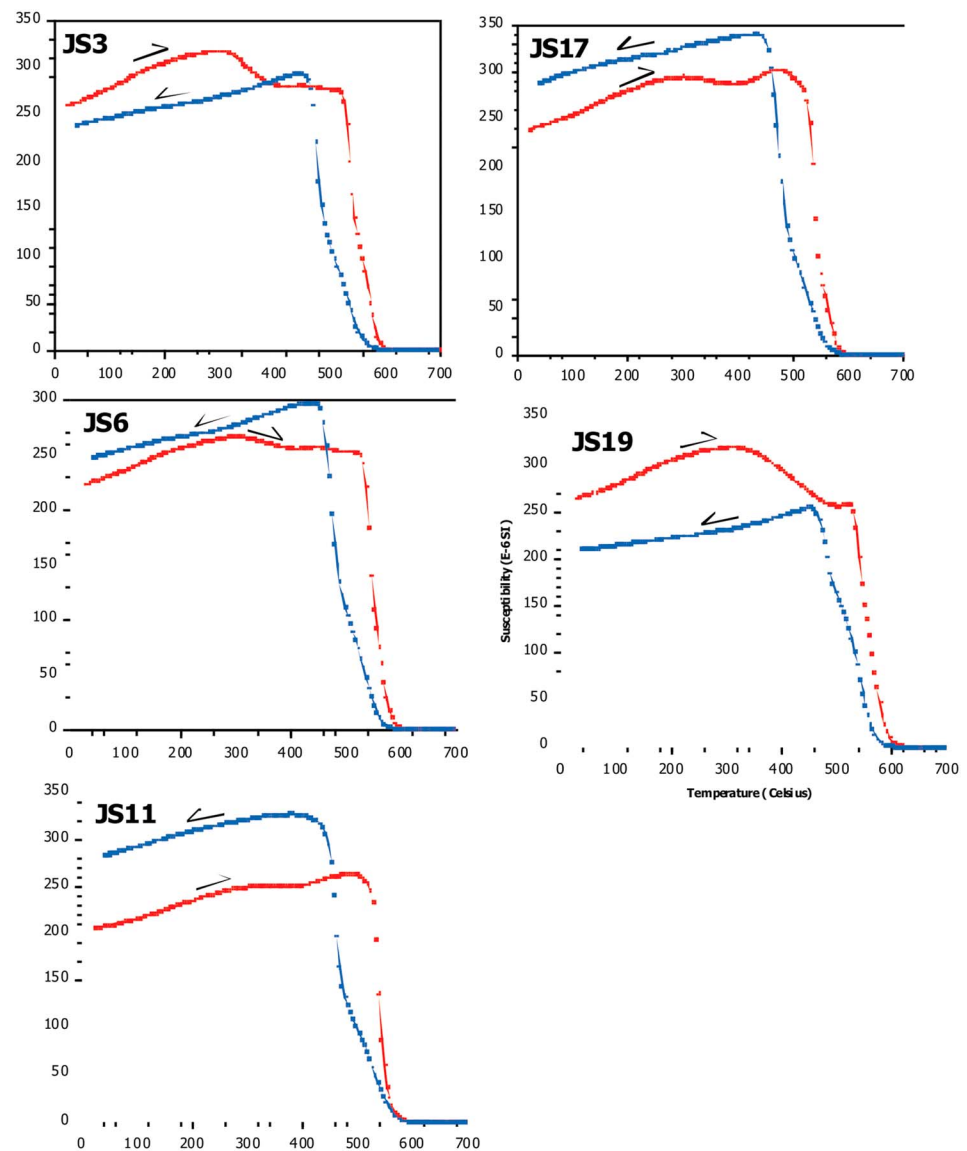
Figure 7. Thermomagnetic curves representing the characteristic magnetic phases in the Jack Springs Tuff. The results are consistent with titanomagnetite with low Ti composition of a PSD grain size. During the cooling stage, the bump is not observed, which can be interpreted to reflect the homogenization of exsolved Fe-Ti oxide phases into a single titanomagnetite phase during the heating, likely course-grained maghemite or an Fe sulfide phase.

observations to currently be in a left-transtensional state (Bennett et al., 1999, 2003; Dixon et al., 2000; Oldow, 2003; Oldow et al., 1994, 2009; Thatcher et al., 1999). A major question remains as to when the region west of the central Mina Deflection evolved and accommodated deformation prior to the initiation of the present-day central Walker Lane system. This study shows that deformation occurred just east of the Sierra Nevada Mountains in the mid-Miocene at the latitude of the Mono Basin. Prior to this study, we did not know that the western Adobe Hills-Southern Huntoon Valley region had experienced deformation resulting in crustal block rotation. This region had been presumed to be undeformed in terms of vertical axis rotation and the area just north of this study area (eastern foothills of the Excelsior Mountains) was used as a presumed unrotated reference location (Petronis et al., 2009). The paleomagnetic results from the Jack Springs Tuff reveal that the regional extent of the area affected by clockwise vertical-axis rotation is not confined to the central Mina Deflection in western Nevada (e.g., Petronis et al., 2009). We show that the area south and east of Huntoon Valley into eastern California has experienced 25° to 104° of clockwise

Table 4
Curie Point Estimates and Titanium Content

Site	Low Temperature Phase[b]	Hopkinson Peak	Inflection Point	Ti Content[c]
JS3	315	517	579[a]	0.060
JS6	330	525	571[a]	0.047
JS11	301	507	546[a]	0.004
JS17	310	478	554[a]	0.006
JS19	331	530	580[a]	0.019

Note. Temperature versus low-field susceptibility experiments provide a quantitative means to estimate mineral composition based on the Curie point when a single magnetic phase is present within the sample (e.g., titanomagnetite). Using the equations from Akimoto (1962) and the titanomagnetite solid solution series, where $Fe_{3-x}Ti_xO_4$ (x = titanium content).
[a]Preferred Curie point. [b]Not present on the cooling curve. [c]Ticontent calculated after Akimoto (1962).

vertical rotation during an "early" phase of displacement transfer in this part of the west-central Walker Lane (Figure 11), consistent with other paleomagnetic studies (Gledhill et al., 2016; Johnson et al., 2014).

Vertical-axis rotations are also found in the area north and west of the Mono Basin (King et al., 2007; Rood et al., 2011; Carlson et al., 2013), an area known as the west-central Walker Lane (Carlson et al., 2013; Faulds & Henry, 2008; Hardyman, 1984; Locke et al., 1940; Stewart, 1988; Surpless, 2008; Wesnousky, 2005; Figure 12). Carlson et al. (2013) presented compelling paleomagnetic data from the Eureka Valley Tuff of the late Miocene Stanislaus Group that defined discrete domains with heterogeneous regional distribution of clockwise vertical-axis rotation, ranging from ~10° to 60° since approximately 9.5 Ma (Figure 12). Rood et al. (2011) documented similar magnitude rotations in that region. Furthermore, preliminary data from Pliocene-age rocks in the Adobe Hills in eastern California and Queens Valley in western Nevada (Grondin et al., 2016; Grondin & Petronis, 2016; Petronis et al., 2015, 2016) show spatially variable components of both clockwise and counterclockwise vertical-axis rotation up to the eastern edge of the Mono Basin. Collectively, these studies demonstrate that the west-central Walker Lane region experienced rigid-block rotation. The well-organized structures in the central Walker Lane and central Mina Deflection facilitated the crustal deformation in that area. However, how and when late Miocene deformation occurred in the Mono Basin and surrounding area is paramount to understanding the tectonic evolution of this region.

7.1. Probable Source Area of the Jack Springs Tuff

Pyroclastic volcanism during the Oligocene to earliest Miocene was intense throughout much of the Western Cordillera and Basin and Range Province (NAVDAT; http://www.navdat.org/). Based on the outcrop characteristics, the Jack Springs Tuff consists of a single cooling unit emplaced during one explosive eruption. Most likely this was a caldera-forming eruption, but the approximate size of the caldera cannot be estimated without directly mapping and reconstructing it, or more accurate information on the overall eruptive volume of the ignimbrite. Furthermore, Miocene fragmentation of the ignimbrite sheet makes identifying the source area particularly difficult. We have identified that the thickest deposits (~50 m) are located near the southern end of Jack Springs Canyon where a near-complete ignimbrite section (basal ground layer (#1) and main body #2a and #2b; Sigurdsson et al., 1999) capped by andesite lava flows is exposed (WGS84; 11S 4217635, 371691). Moving north, west, and east from the Jack Springs Canyon section the ignimbrite thins. The outcrops in the Bodie Hill reference location are volumetrically sparse, occur on presumed
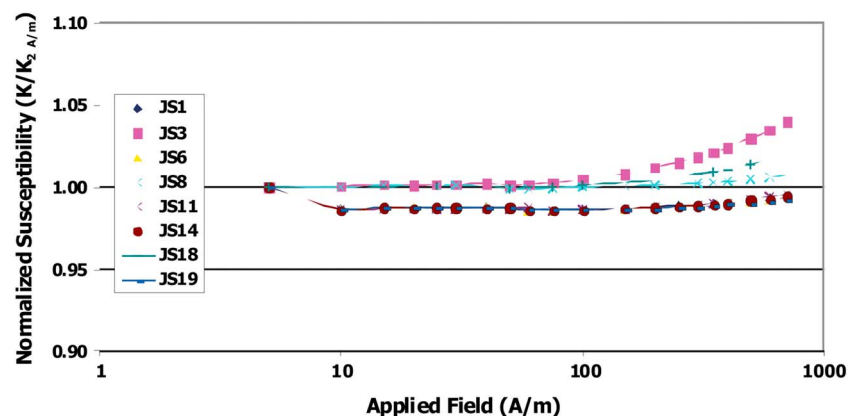

Figure 8. Magnetic susceptibility normalized to a 2-A/m applied field as a function of field amplitude. All samples show little field dependence on susceptibility indicating a low Ti content of the titanomagnetite phase.
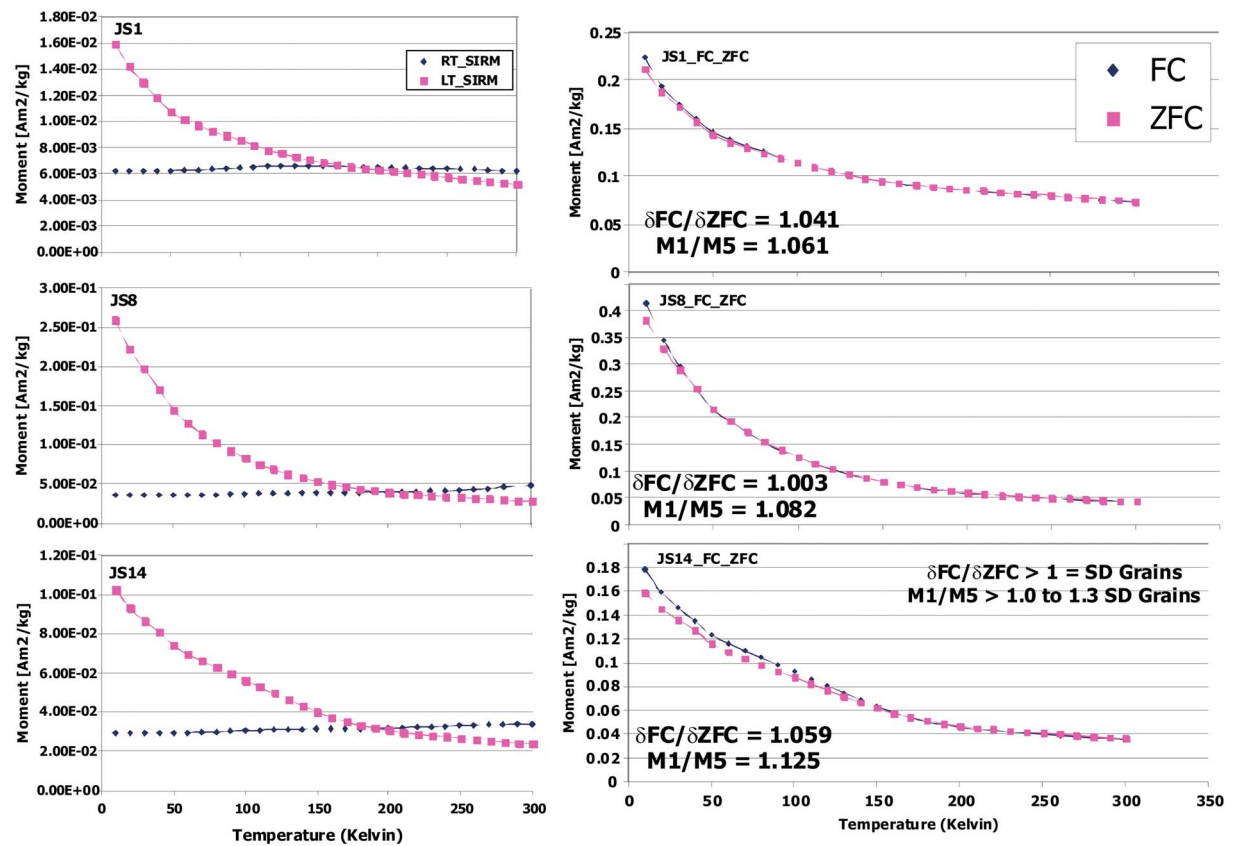
Figure 9. Magnetic property measurement experiments. (a–c) Room temperature saturation isothermal remanent magnetization (RT_SIRM) and low-temperature SIRM (LT_SIRM) experiments. The three samples show little to no dependence on temperature on cooling indicative of ferromagnetic ordering behavior. The large initial remanence on the warming curve is the LTSIRM and does not reflect a paramagnetic component. (d–f) Field cooled (FC) and zero-field cooled (ZFC) remanence on warming experiments. The three samples show little to no dependence on temperature indicative of ferromagnetic ordering behavior. The ratio of the δFC/δZFC and the ratio of M1/M5 provide an estimate of the magnetic domain state indicative of single-domain grains.

basement highs, and are thin unwelded distal outflow facies of the ignimbrite (John et al., 2015). The new AMS data we report here are interpreted to indicate a probable northward transport direction for the Jack Springs Tuff with the source area located to the south of the study area (Appendix B). The area south of Jack Springs Canyon is locally referred to as the southern Huntoon Mountains and Queens Valley region. The area south of Huntoon Valley is characterized by roughly northeast-southwest trending faults that swing south-southeast as they enter the northern Queens Valley region (Gilbert et al., 1968; Stewart, 1981). The faults fragment Tertiary olivine basalts, latite ignimbrite, and trachyandesite flows into discrete structural blocks. Small releasing bend pull-apart basins occur were the faults change orientation and are filled with Quaternary alluvium. Locally, throughout the region structural windows occur that reveal Paleozoic and Precambrian basement rocks.

Numerous AMS studies of silicic pyroclastic rocks demonstrate that the source area of ignimbrite sheets can be approximated by triangulation with AMS fabric data from adequately distributed sampling locations (e.g., Alva-Valdivia et al., 2005; Ellwood, 1982; Knight et al., 1986; MacDonald & Palmer, 1990; Ort et al., 1999; Wolff et al., 1989). Many of these studies use the K_1 lineation as a proxy for the magma flow direction when the magnetic fabric is dominantly prolate or for oblate fabrics when the K_1 lineations are statistically well grouped from dispersed sites. The AMS data from the Jack Springs Tuff all yield oblate-shaped magnetic fabrics with no consistent trend in the K_1 lineation (Table 2 and Appendix B). In order to interpret the transport direction from the Jack Springs Tuff, we used the imbrication of the magnetic foliation plane (Ellwood, 1982; Knight et al., 1986). Knight et al. (1986) showed that a flow sense can be extracted from AMS data based the magnetic foliation plane. Their study of oriented thin sections revealed a small (between 10°
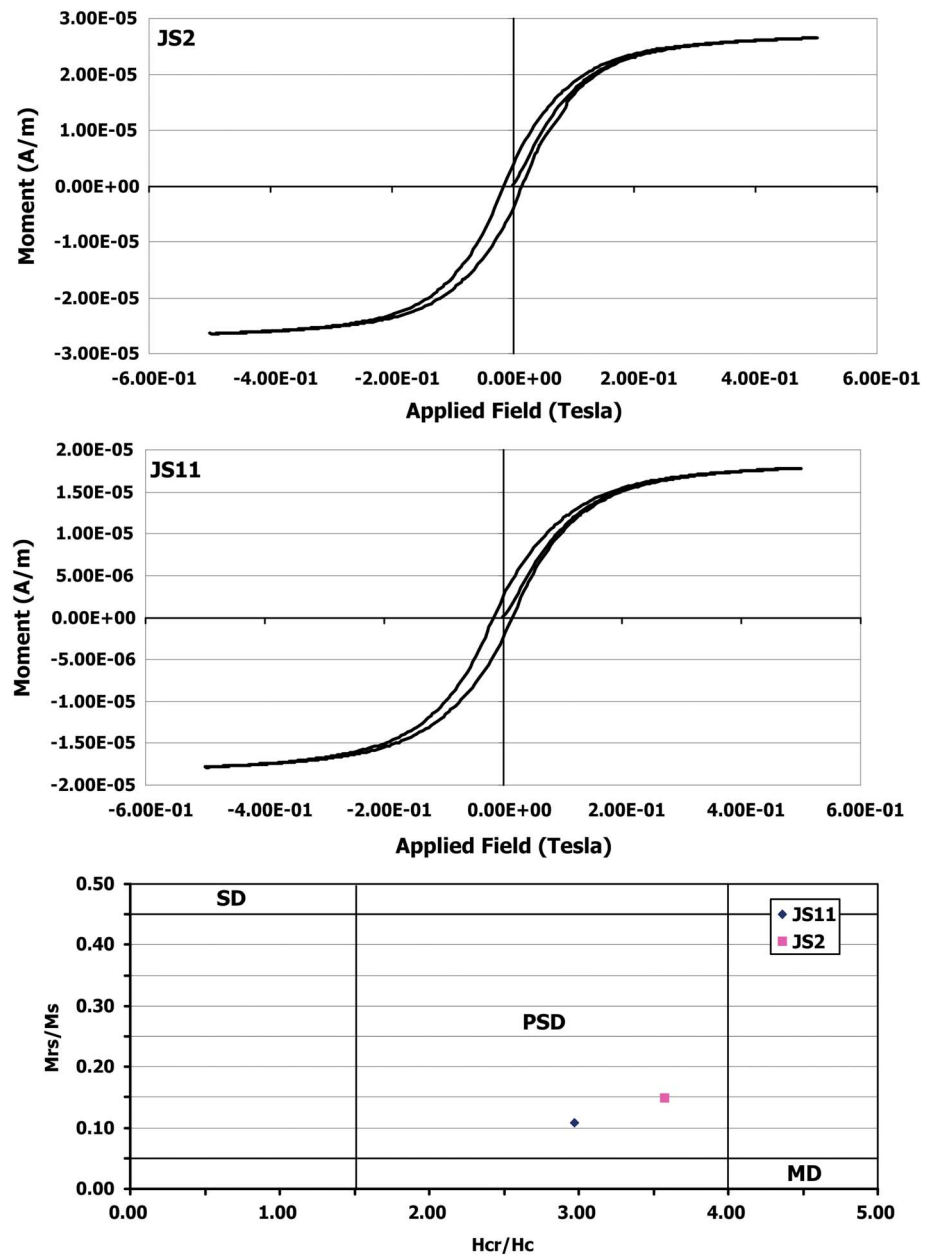
Figure 10. Hysteresis data. (a and b) Hysteresis curves for two samples of the Jack Springs Tuff. The shapes of the curves are consistent with a single-domain to pseudodomain grain size for a ferromagnetic material. (c) Day plot. Mr, remanent magnetization; Ms, saturation magnetization; Hc, intrinsic coercivity; Hr, coercivity of remanence.

and 30°) sourceward dipping imbrication of the magmatic foliation consistent with the magnetic fabric. Several other AMS studies of ash flow tuffs have shown that the magnetic foliation plane dips toward the source region (Lamarche & Frogatt, 1993; MacDonald & Palmer, 1990; Ort, 1993; Palmer et al., 1991; Seaman et al., 1991). The mean imbrication of the magnetic foliation, corrected for tilt and vertical axis rotation, trends toward 178° and the magnetic foliation plane dips 10.3°S and strikes 079.8° (Appendix B). The overall pattern of AMS magnetic foliation and AMS triangulation data leads us to speculate that the likely source region, and hence, the Jack Springs Tuff caldera is probably located near or within the southern Huntoon Mountains and Queens Valley region (Appendix B). It is important to note that the AMS triangulation directions, corrected for structural tilt and vertical axis rotation, do not converge on a
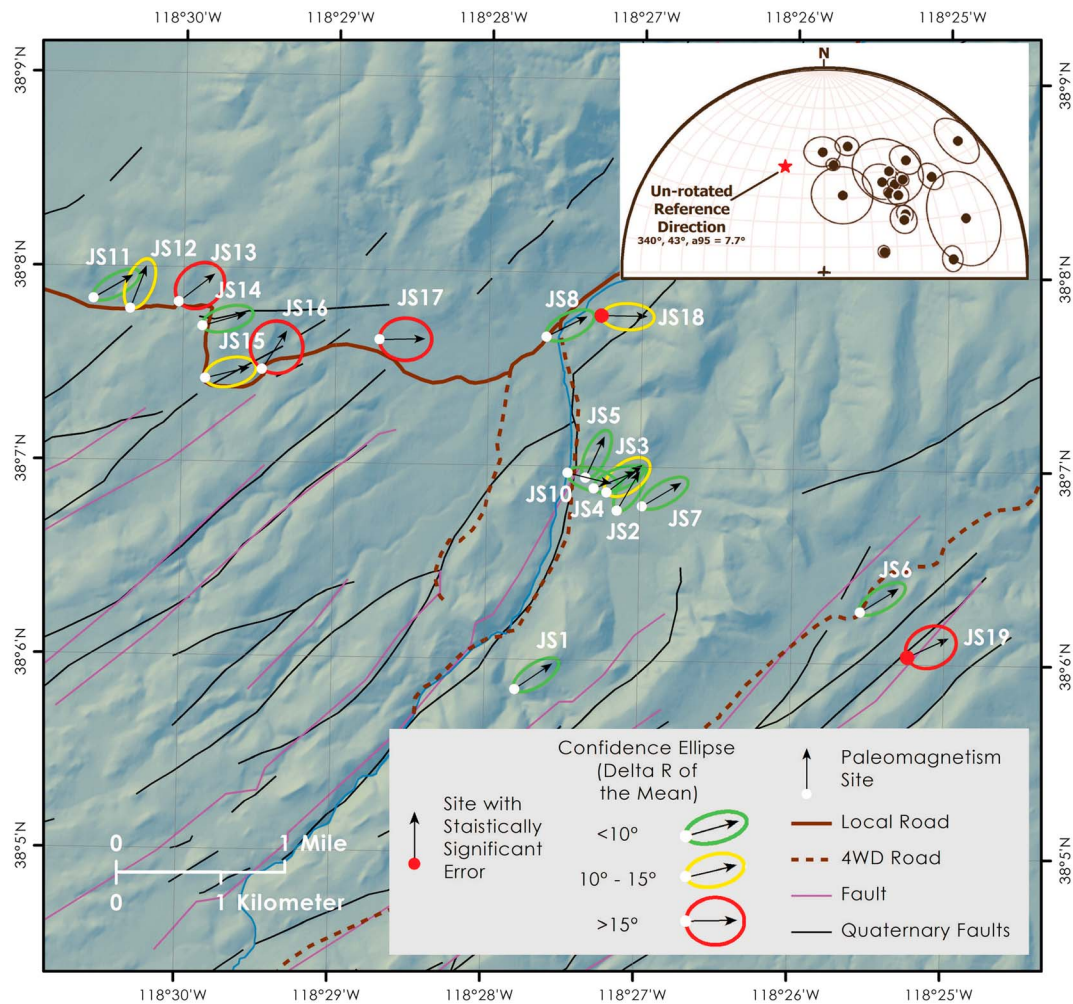
Figure 11. (a) Summary map of all paleomagnetic data from the Jack Springs Tuff. Each arrow represents a paleomagnetic sample location. Any deviation of the arrow from north indicates a vertical axis rotation (R) relative to the reference location in the Bodie Hills, CA (Figure 2). The confidence ellipse about the arrow represents the delta R of the mean (see Table 3). The short axis of the ellipse is equal to the delta R error; the long axis is of arbitrary length (see Appendix D). Sites JS18 and JS19, highlighted with a red dot, yield rotations that are suspect due to inclination anomalies (i.e., the site yields a statistically significant flattening (F) estimate that is greater than 10° of the delta F error estimate). As discussed in the text, poorly defined paleohorizontal information likely contributes to the high inclination deviation. (b) Inset: lower hemisphere equal area projection of site mean paleomagnetic data from the Jack Springs Tuff with α95 confidence ellipse about the site mean direction (Fisher, 1953). The red star is the reference direction in the Bodie Hills used to calculate rotation estimates.

unique location. The majority of the directions trend to the southeast and southwest, and thus, we hypothesize that the source vent is likely located in this general direction.

7.2. Implications of the Jack Springs Tuff Paleomagnetic Data

The paleomagnetic data from the Jack Springs Tuff, when compared with respective data from the reference section in the western Bodie Hills, reveal declination discrepancies, and thus inferred vertical-axis rotation of structural blocks. Rotation estimates average +59.7° ± 22.8° and range from +25° to +104° (+ indicates a clockwise rotation; Figure 11 and Table 3). Close inspection of the data reveal that three sites yield anomalously high rotation estimates (JS10–104.1°, JS17–89.0°, JS18–91.1°). The results from these sites are difficult to reconcile with the other sites from nearby structural blocks. The rotation estimates from these three sites are unrealistically high, and would require very large strain gradients between fault blocks and no such field evidence was observed; we consider these rotation estimates anomalous. As discussed earlier, we selected the region near the eastern escarpment of the Sierra Nevada as our reference location, since this region is hypothesized (Carlson et al., 2013) to have experienced low rotation (< +13°). It is
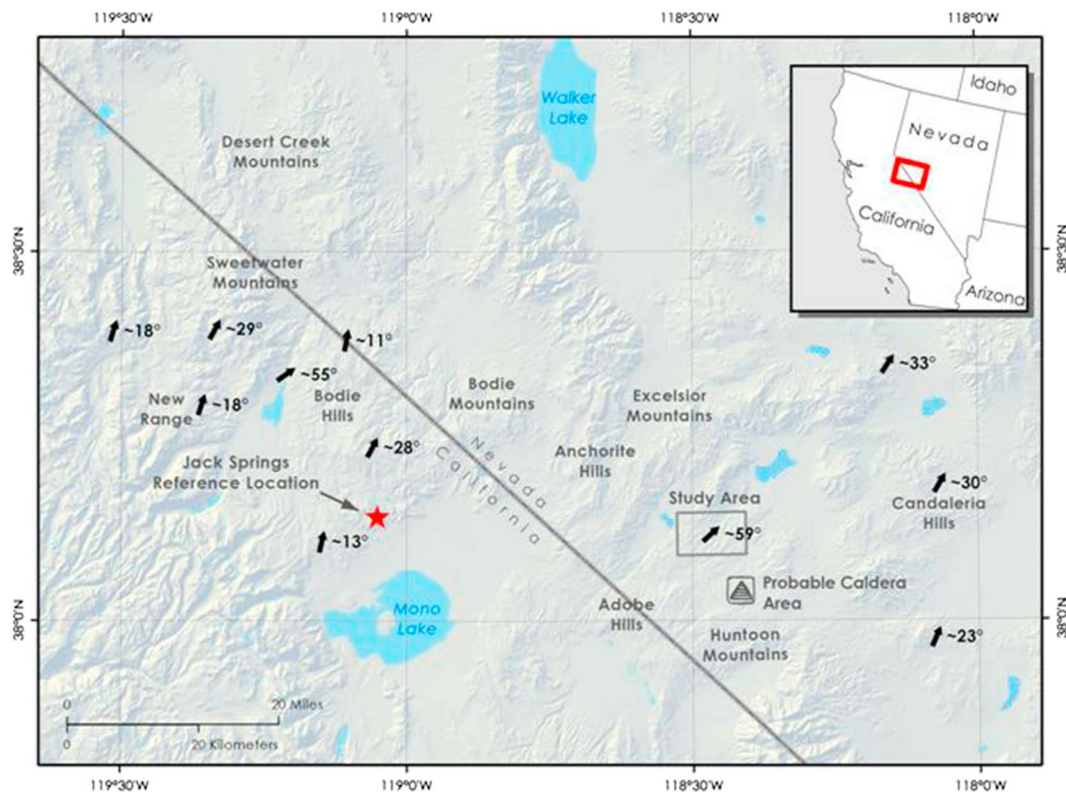
Figure 12. Summary map of the published and new paleomagnetic data from the eastern Sierra Nevada escarpment, CA, to the Monte Cristo Range, NV, at the approximate latitude of Mono Lake. The arrows indicate the inferred vertical axis rotation as either absolute rotation values relative to an established paleomagnetic pole or a relative rotation referenced to a fixed location. The probable caldera that erupted the Jack Springs Tuff is indicated in the southern Huntoon Mountains-Queens Valley region south-southeast of the study area.

important to note that the rotation estimates from the Jack Springs Tuff in the western Mina Deflection are considerably greater than previous results from the central Mina Deflection (Petronis et al., 2009). The relative rotation data in the central Mina Deflection region from three late Oligocene regional ignimbrites and absolute rotation estimates from multiple sequences of mid-Miocene andesite flows and late Miocene to Pliocene basalt flows yielded statistically indistinguishable average rotation estimates of +21° ± 10° and +27° ± 8°, respectively. Previous paleomagnetic investigations in the Silver Peak Range (east to northeast area, Petronis et al., 2002; southwest area, Petronis et al., 2007) have shown that Miocene volcanic rocks in the upper plate of the northwest dipping Silver Peak-Lone Mountain detachment system (as well as Miocene mafic intrusions in the lower plate) have experienced net clockwise rotation of some 25°. These collective data led Oldow et al. (2008) and Petronis et al. (2009) to hypothesize that the rotations in the Silver Peak Range as well as those inferred to have affected the Candelaria Hills and adjacent areas were the manifestation of a broad zone of "early" (late Miocene to earliest Pliocene) deformation phase. We argue that this phase postdates Miocene deformation in the Mono Basin region. We interpret the higher rotation estimates from the Jack Springs Tuff to reflect the net rotation across the area since the middle Miocene, while the vertical-axis rotation in the central Mina Deflection area is likely latest Miocene to earliest Pliocene in age. The documentation of the high net rotation in the study area is consistent with one hypothesis that deformation was being accommodated by vertical axis rotation over an extended period that began earlier than originally hypothesized (Oldow et al., 1994).

7.3. Evolution of the Western Mina Deflection

Interpretation of the ancient to present-day deformation rates of the west-central Walker Lane varies among researchers and the data sets that they use to estimate the rates. Paleomagnetic estimates from

early to middle Miocene age material constrain rotation rates of ~5° ± 2°/Myr (Rood et al., 2011). Other studies, however, interpret the data to indicate spatially and temporally varying rates (see Carlson et al., 2013 for a review). In both cases, these rates are inconsistent with present-day geodetic models that calculate present-day vertical-axis rotation rates of ~1°/Myr or less (e.g., Hammond et al., 2011; McCaffrey, 2002). However, new GPS-based models proposed by Bormann et al. (2016), predict present-day block rotation rates in the central Walker Lane that vary spatially across the region. Their preferred model constrains present-day clockwise block rotation rates of about 2.0–2.5°/Myr in the Mina Deflection and lower rotation rates between 1.1 and 1.3°/Myr in the Bodie Hills (Figure 2). Quaternary faults in the Adobe Hills, southern Huntoon Mountains, and Queens Valley show predominantly dip-slip motion within the west-central Walker Lane that is kinematically incompatible with vertical-axis rotation. The older structures that are cut by the Quaternary faults often show transtensional offsets consistent with accommodating vertical axis rotation (Hogan, 2011; John et al., 2015; Lee et al., 2009; Nagorsen-Rinkel et al., 2013). The lack of currently active strike-slip faults in the west-central Walker Lane requires that we develop a hypothesis that is different from other regions in the Walker Lane (e.g., active sinistral faulting in the central Mina deflection; Petronis et al., 2009). Carlson et al. (2013) proposed a model of vertical axis rotation within discrete domains and associated edge effects related to transtensional deformation and basin development. This model differs significantly to the models of deformation in the central Mina Deflection (Jayko & Bursik, 2012; Oldow et al., 2001, 2008; Petronis et al., 2009; Wesnousky, 2005; Wesnousky et al., 2012).

Here we argue that the region between the Excelsior Mountains and White Mountains served, and continues to serve, as a "zone of weakness" to funnel deformation across the Mono Basin into the central Mina Deflection due to crustal anisotropy (Figure 2). Recent and historic magnetic and gravity data in the area between Excelsior Mountain and the White Mountain structural blocks show gradients in both total field magnetic and isostatic residual gravity data (Bursik et al., 2003; Christensen et al., 1969; Gilbert et al., 1968; McDonell, 2013; Pakiser et al., 1960; Roberts & Jachens, 1999). A pronounced magnetic high occurs just west of the Adobe Hills (Adobe Flats) at the California-Nevada border that increases rapidly into the western Mina Deflection just south of Huntoon Valley (Appendix Ca). The regional aeromagnetic anomaly map of the area (McDonell, 2013) shows a significant increase in total magnetic field from around +65 nT in the Adobe Flats to over +250 nT just south of Huntoon Valley across the Jack Springs Canyon sampling area (Appendix Ca). To the north, a magnetic low extends from north of Mono Lake well into western Nevada into the central Mina Deflection where the total field intensity drops from +250 to less than −230 nT (McDonell, 2013). In the same area, isostatic residual gravity data increase from ~20 mGal in the Adobe Flats to about 30 mGal in the area just south of Huntoon Valley; consistent with the magnetic data (McDonell, 2013; Appendix Cb). These rapid, abrupt changes in magnetic and gravity data may reflect a fundamental change in the shallow to midcrust between the Excelsior and White Mountain structural blocks. We speculate that this change may facilitate deformation through displacement transfer across this region.

Assuming a constant rate of rotation for the Jack Springs Tuff sampling area yields an average rotation rate, since 12.1 Ma, of 4.9° +/− 1.9°/Myr. This rotation rate is consistent with previous paleomagnetic observations in deformed areas. Petronis et al. (2009) documented inferred rotation of the upper and lower plate rocks in the Silver Peak Range from ~4° to 8°/Myr. Sonder et al. (1994) argued for rotation rates between 1° and 12°/Myr in their study of Miocene strata in the Gale Hills near the Las Vegas Valley shear zone. Rowan and Roberts (2008) inferred a rotation rate between 7° and 14°/Myr for early Miocene deformation and a decreased rotation rate of 3°–4°/Myr in the Quaternary on the North Island of New Zealand. In the area further west and north across the Mono Basin (Figure 2), the lack of statistically significant rotation in Pliocene volcanic rocks supports a hypothesis of present-day low or no rotation in the Bodie Hills region (Carlson et al., 2013) consistent with geodetically determined present-day rotation rates (~1 /Myr). In terms of "constant" rotation rates based on the Jack Springs Tuff, we argue that the rate is likely unrealistic given the range of rotation estimates from the tuff (Table 3). Based on the paleomagnetic data, the individual fault blocks sampled experienced variable degrees of clockwise rotation and we cannot use the Jack Springs Tuff to estimate robust rotation rates. We can, however, use the data to establish that the region experienced clockwise rotation, and the variability is related to distributed shear across the region.

Detailed mapping in the Adobe Hills reveal the dominance of northeast striking sinistral faults and a smaller population of northwest striking dextral faults (Nagorsen-Rinkel et al., 2013; Figure 2). Pliocene-age rocks in the Adobe Hills in eastern California and southern Huntoon Mountains-Queens Valley in western Nevada yield components of both clockwise and counterclockwise vertical axis rotation attesting to post-Pliocene deformation up to the eastern edge of the Mono Basin (Petronis et al., 2015; Grondin et al., 2016; Grondin & Petronis, 2016; Petronis et al., 2016). The vertical axis rotation documented in this area and published fault kinematic data based on fault geometries are interpreted to indicate that deformation across this part of the western Mina Deflection is characterized by a simple shear couple leading to fault block rotation. A simple shear couple is a block rotation model in which slip along connecting faults, combined with vertical axis rotation of intervening fault blocks, transfers fault slip across the zone of deformation to accommodate displacement transfer (modified from McKenzie & Jackson, 1983, 1986; Wesnousky, 2005). Fault blocks that are bounded by sinistral faults yield clockwise rotations while blocks bounded by dextral faults yield counterclockwise rotations. Geologic studies further south centered on sinistral Quaternary faults in the Queen Valley area, however, did not yield evidence for recent clockwise block rotation (Lee et al., 2009). We argue that deformation related to slip transfer across the region is focused in the area between the Excelsior Range and the northern White Mountains (Figure 2). The area around Queens Valley (Lee et al., 2009) does not appear to have been effected by the deformation we document to the north.

We pose the hypothesis that vertical-axis rotation varied spatially and temporally and argue that the region from the eastern Mono Basin through the Adobe Hills into the southern Huntoon Mountains and northern Queens Valley has facilitated displacement transfer since at least the mid-Miocene. We note that Lee et al. (2009) showed that Quaternary age structures in southern Queens Valley do not show evidence of vertical axis rotation. Rather, they argue that dextral fault slip is transferred by both a restraining westward step and a releasing eastward step. The dextral shear being transferred from the White Mountains-Owens Valley fault zone has been partitioned into the region that is bounded by the Excelsior Mountain block to the north and the White Mountain block to the south (Figure 12). During the mid-Miocene, deformation in the Bodie Hills relaxed resulting in the growth of structures consistent with the new stress field. This was most likely due to changes in plate boundary stresses as evidenced by mineralized veins and faulting within the Bodie Hills (John et al., 2012). The kinematic indicators used by John et al. (2012) include fault breccias, mineralized zones crisscrossed by hairline silica veinlets, hematite-stained conjugate fractures, banded quartz veins with millimeter- to centimeter-scale bands with inward facing crystal terminations indicative of repeated tensional fracturing (John et al., 2012). John et al. (2012) argued that the change in the regional stress field was due to the migration of the Mendocino Triple Junction inferred to have been at the latitude of the central Walker Lane by about 10 Ma (~38°N; Atwater & Stock, 1998; Jones et al., 2004; see discussion by Carlson et al., 2013). Following the change in stress field, deformation became focused in a zone of crustal weakness/crustal anisotropy between the Excelsior Mountain and the White Mountain blocks (Appendix C).

7.4. Tectonic Development of the Western Mina Deflection

Three simplified models have been proposed to explain the fault geometries and kinematics that accommodate displacement transfer into the central Mina deflection. These include (1) the displacement-transfer model (Oldow, 1992a, 1992b; Oldow et al., 1994), (2) the transtensional model (Oldow, 2003), and (3) the simple shear couple model (modified from McKenzie & Jackson, 1983, 1986; Wesnousky, 2005). In the displacement-transfer model, normal slip occurs along connecting faults between the bounding regional dextral fault systems on the west and east sides of the central Mina deflection, while in the transtensional model the connecting faults accommodate deformation via sinistral and normal slip. The simple shear couple model envisions oblique sinistral normal slip along the connecting faults with components of clockwise vertical axis to accommodate the displacement transfer (Figure 13).

This study shows that deformation occurred south of Huntoon Valley via oblique sinistral slip and clockwise vertical axis rotation in a region that had been presumed to lack vertical axis rotation (Oldow et al., 1994; Petronis et al., 2009). The results from this study are best explained by a modified version of the simple shear couple model (McKenzie & Jackson, 1983, 1986; Wesnousky, 2005). We document that individual structural blocks have rotated nonuniformly across the study area and attribute this deformation style to
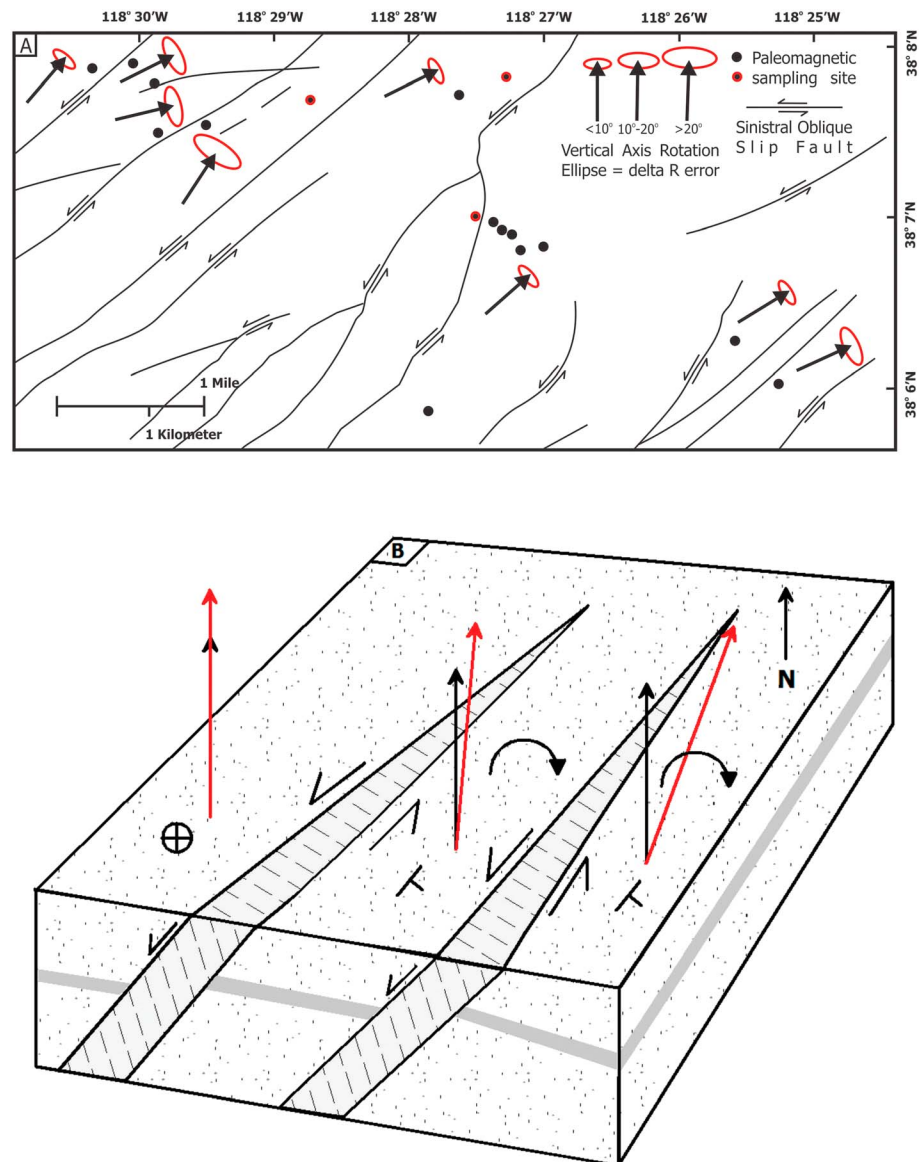
Figure 13. Tectonic development of southern Huntoon Valley. (a) Vertical axis rotation averages within each structural block based on paleomagnetic data from the Jack Springs Tuff. The faults are pre-Quaternary structures that demonstrate sinistral oblique motion with variable amounts of offset based on historic mapping (Gilbert et al., 1968; Stewart, 1981). Arrows with ellipse represent the average amount of vertical axis rotation (R) with respect to the reference section in the Bodie Hills, CA, for the individual structural block. The red ellipse is a schematic representation of the delta R error based on the data from Table 3. Black circles are paleomagnetic sampling sites. Red circles with black centers are sites with unrealistically high rotations estimates (> ~90°; see text for discussion), and these three sites are not included in the block rotation estimates. Any deviation of the arrow from north indicates a vertical axis rotation. (b) Schematic block diagram depicting a simple shear couple and the resulting vertical axis rotation and horizontal axis tilting. The red arrows depict a schematic vertical axis rotation with respect to the reference location.

distributed shear in the upper brittle and ductile lower crust since the mid-Miocene (Figure 13a). The pre-Quaternary structures accommodated distributed shear along sinistral oblique slip faults resulting in components of modest horizontal axis tilting and variable amounts of vertical axis rotation related displacement transfer from the western Mina defection into the evolving central Mina deflection and Silver Peak-Lone Mountain detachment system (Figure 13b). We argue that this displacement transfer system was active in the mid-Miocene and by late Miocene-Pliocene deformation stepped east into the

organized structures of the central Mina deflection and Silver Peak-Lone Mountain detachment system accommodating the deformation. The significant net rotation in this part of the western Mina deflection, relative to other areas in the vicinity, is interpreted to indicate that deformation was accommodated over an extended period of time that began earlier than originally hypothesized (Oldow et al., 1994). Carlson et al. (2013) pointed out that an eastward increasing amount of vertical axis rotation occurred from the eastern Sierra Nevada front into the Bodie Hills and western Mina deflection. They argued that this could be explained by a quasi-continuum model (e.g., Sonder et al., 1994), wherein the magnitude of rotation increases moving toward the center of the deforming region (i.e., the Walker Lane). The deformation in the western Mina deflection observed in the paleomagnetic data from the Jack Springs Tuff (Figures 13a and 13b) reflects that the brittle upper crust is likely coupled to ductile shearing at depth. The deformation reflects distributed shear between the Excelsior and White Mountain structural blocks along a zone of crustal weakness (Appendix C). In the central Mina deflection, late Miocene to recent deformation is partitioned across the region via both wrench-dominated and extension-dominated transtension, and modest vertical axis rotation of about 20°–30° since the late Miocene (Oldow et al., 2008; Petronis et al., 2009; Wesnousky, 2005). Present-day physiographic fault patterns allude to an abrupt transfer system boundary and Global Positioning System data (Bennett et al., 2003; Dixon et al., 2000; Oldow et al., 2009) as well as recent structural and mapping studies further indicate that the deformation extends to the west and east of the modern Mina deflection (Lee et al., 2009; Hogan, 2011; Nagorsen-Rinkel et al., 2013; Carlson et al., 2013).

Tectonic boundaries of many modern transfer systems appear clear on inspection (e.g., Condie, 2016), yet the true extent of the systems remain elusive, and the timing of when parts of these systems were active remains poorly constrained. On a global scale, documenting the heterogeneous deformation that is observed in the western and central Mina deflection and surrounding region provides critical data on the evolution of long-lived transtensional fault systems. The available paleomagnetic data in the western Mina deflection and adjoining region arguably extend the area affected by modest magnitude vertical-axis rotation, presumably associated with transfer zone development, and define a region much larger than previously expected during the mid-Miocene. Paleomagnetic, structural, and geodetic studies support a transition from more diffuse to localized deformation forming the central Mina deflection at about 3 Ma (Jones et al., 2004; Oldow, 2003; Oldow et al., 1994, 2008; Petronis et al., 2009). Future questions to address include (1) what is the mechanism by which generally northwest striking faults transfer slip from the northern Eastern California Shear Zone to the central Walker Lane Belt?; (2) is slip transfer dominated by left-lateral strike-slip faulting and clockwise block rotation, dip-slip normal faulting, or some combination of the two mechanisms?; (3) what factors control the mechanism by which slip is transferred?; and (4) when did transtensional deformation step east into the present-day central Mina deflection? Although we cannot address all these questions, our data allow us to place limitations on the mechanism of slip transfer in the region. We argue that oblique sinistral slip and clockwise vertical axis rotation in the western Mina deflection accommodated the deformation in agreement with the results summarized by Carlson et al. (2013) further west of our study area. Based on the magnitude of the vertical axis rotation, deformation occurred in the western Mina deflection during the mid-Miocene prior to the initiation of the structures in the central Mina deflection. In addition, our results provide data that can be used by the geodynamics community to further develop and refine regional and global intracontinental deformation models.

8. Conclusions

The results from this study are interpreted to support a new model in which the area between the Excelsior Mountain and White Mountain structural blocks appears to act as a "zone of weakness" in which deformation has been partitioned from the White Mountains-Owens Valley fault zone across the eastern Mono Basin into the central Mina Deflection. Magnetic and gravity data between the Excelsior Mountain and the White Mountain structural blocks reveal gradients in both total field magnetic and isostatic residual gravity data. We argue that a fundamental change in the shallow to midcrust exists that facilitates deformation through displacement transfer across this region. Paleomagnetic rotation estimates from the Jack Springs Tuff reveal spatially variable components of clockwise vertical axis rotation that range from 25° to 104° with an average rotation of 59.7° ± 22.8°. These data are consistent with results from locations further to the west and north that have documented similar magnitude rotation estimates. The

paleomagnetic results from the western Mina Deflection are significantly greater than the rotation estimates from the central Walker Lane and likely reflect a protracted period of block rotation. Rock magnetic data indicate that the dominant magnetic mineral phase is a cubic Fe-Ti oxide phase likely titanomagnetite of a restricted grain size of psuedosingle domain. A new $^{40}Ar/^{39}Ar$ age determination places the eruption of the Jack Springs Tuff at 12.114 ± 0.006 Ma. The anisotropy of magnetic susceptibility data place a probable, roughly northward transport direction for the Jack Springs Tuff from a buried caldera located in the southern Huntoon Mountains and Queens Valley region. This supposition is supported by field observations that indicate that the thickest part of the ignimbrite observed is exposed in its near complete thickness of ~50 m at the southern end of Jack Springs Canyon. The ignimbrite thins to the north, east, and west, outcropping as only sparse, poorly welded deposits in the Bodie Hills, CA. The results from this study highlight a protracted period of deformation in a region that was thought to have experienced minimal crustal block rotation associated with strike-slip faulting east of the Sierra Nevada Mountain Range. We interpret the results from our paleomagnetic study to indicate that the western Walker Lane has accommodated deformation related to North American-Pacific plate interactions since at least the middle Miocene and presently serves as a relay zone to partition deformation across the central Mina Deflection and into the northern Walker Lane.

Appendix A: Summary of 40Ar/39Ar Results and Analytical Methods

A1. Sample Preparation and Irradiation

Minerals separated with standard heavy liquid, Franz magnetic, and hand-picking techniques. Samples in NM-284 irradiated in a machined aluminum tray for 16 hr in C.T. position, USGS TRIGA, Denver, CO. Neutron flux monitor Fish Canyon Tuff sanidine (FC-2). Assigned age = 28.201 Ma (Kuiper et al., 2008).
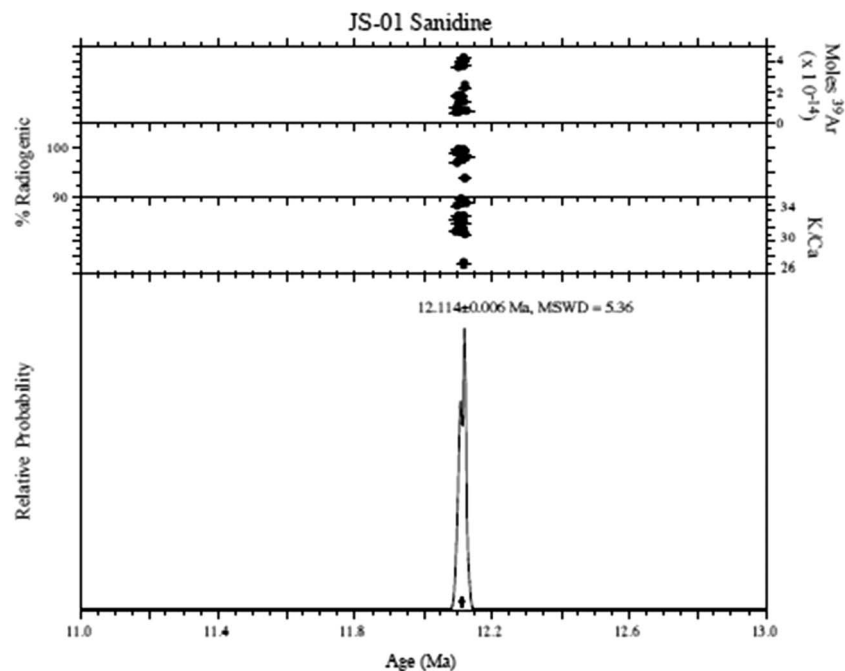

Figure A1. Age probability distribution diagram (ideogram). The lower plot, apparent age (x axis), is plotted versus the summation of the normal distribution of each individual analysis. This is roughly comparable to a histogram plot. The auxilliary plots include moles of 39ArK released per crystal, radiogenic yield, and K/Ca ratio, as well as the age ± error for the individual data points.

Table A1
40Ar/39Ar Analytical Data

ID Power (watts)	40Ar/39Ar	37Ar/39Ar	36Ar/39Ar (x 10-3)	39ArK (x 10-15 mol)	K/Ca	40Ar*(%)	Age (Ma)	±1σ (Ma)
JS-01, Groundmass, J=0.0039305±0.02%, IC=0.9990071±0.0017945, NM-284D, Lab#=65098, Argus VI
13 3.5	1.715	0.0164	0.0745	6.397	31.2	98.8	12.097	0.006
02 3.5	1.716	0.0147	0.0728	15.951	34.7	98.8	12.102	0.004
12 3.5	1.751	0.0155	0.1939	8.967	32.9	96.8	12.103	0.007
06 3.5	1.706	0.0158	0.0380	32.905	32.2	99.4	12.106	0.002
03 3.5	1.705	0.0153	0.0347	6.376	33.3	99.5	12.107	0.005
04 3.5	1.718	0.0143	0.0774	36.145	35.6	98.7	12.112	0.003
10 3.5	1.738	0.0161	0.1434	12.322	31.7	97.6	12.113	0.005
09 3.5	1.724	0.0162	0.0972	16.890	31.5	98.4	12.114	0.004
08 3.5	1.733	0.0157	0.1236	12.707	32.5	98.0	12.119	0.004
11 3.5	1.709	0.0144	0.0424	37.088	35.4	99.3	12.121	0.002
05 3.5	1.726	0.0153	0.1000	34.021	33.3	98.3	12.121	0.003
01 3.5	1.726	0.0189	0.0983	38.667	27.0	98.4	12.122	0.003
07 3.5	1.817	0.0166	0.4054	21.871	30.8	93.4	12.124	0.005
14 3.5	1.736	0.0146	0.1285	7.093	35.0	97.9	12.130	0.006
Mean age ± 2σ	**n=14**		**MSWD=5.36**	**32.6 ±4.5**		**12.114**	**0.006**	

A2. Instrumentation

Total fusion analyses performed on an Argus VI mass spectrometer on line with automated all-metal extraction system. System = Jan. Multicollector configuration: ^{40}Ar-H1, ^{39}Ar-Ax, ^{38}Ar-L1, ^{37}Ar-L2, ^{36}Ar-CDD. Flux monitors fused with a Photon Machines Inc., CO_2 laser. Multicollector configuration Obama: ^{40}Ar-H1, ^{39}Ar-Ax, ^{38}Ar-L1, ^{37}Ar-L2, ^{36}Ar-L3; H1, L2, L3 all 10e12 Ohm resistors; AX 10e13 Ohm resistor, L3-CDD Ion counter-deadtime 10 nS. Multicollector configuration Felix: ^{40}Ar-H2, ^{39}Ar-H1, ^{38}Ar-AX, ^{37}Ar-L1, ^{36}Ar-L2, H2, H1, AX, L1 all 10e12 Ohm resistors, L2-CDD Ion counter-deadtime 20 nS.

A3. Analytical Parameters

Sensitivity for the Helix MCPlus with the diode laser = 2.5e − 16 moles/fA. Sensitivity for the ARGUS VI with the diode laser = 1.0e − 16 moles/fA. Typical system blank and background for groundmass 9 ± 2%, 0.3 ± 25%, 0.3 ± 35%, 0.2 ± 100%, 0.04 ± 4.5% x 10–17 moles at masses 40, 39, 38, 37, and 36, respectively. Typical system blank and background for hornblende: 15 ± 8%, 0.03 ± 100%, 0.03 ± 100%, 0.2 ± 20%, 0.09 ± 11% × 10–17 moles at masses 40, 39, 38, 37, and 36, respectively. Typical system blank and background was 83.9, 1.32, 0.499, 0.382, 0.320 × 10^{-18} moles at masses 40, 39, 38, 37, and 36, respectively, for the laser analyses. J factors determined by CO_2 laser fusion of six single crystals from each of eight radial positions around the irradiation tray. Decay constants and isotopic abundances after Min et al. (2000). Multiple blanks are run at the beginning, during, and after step-heating analyses. Blanks are fit with time series analysis and are reported as mean ± standard deviation. Isotope evolutions for ^{40}Ar, ^{39}Ar, and ^{36}Ar are fit with parabolic regression, whereas ^{38}Ar and ^{37}Ar use linear regression. Time zero equals the time of mass spectrometer ion pump closure. Equilibration times: Obama = 15 s, Felix = 30 s. J factors determined by CO_2 laser fusion of six single crystals from each of eight radial positions around the irradiation tray. 40-K decay constant 5.463e − 10/a (Min et al., 2000) (Figure A1).

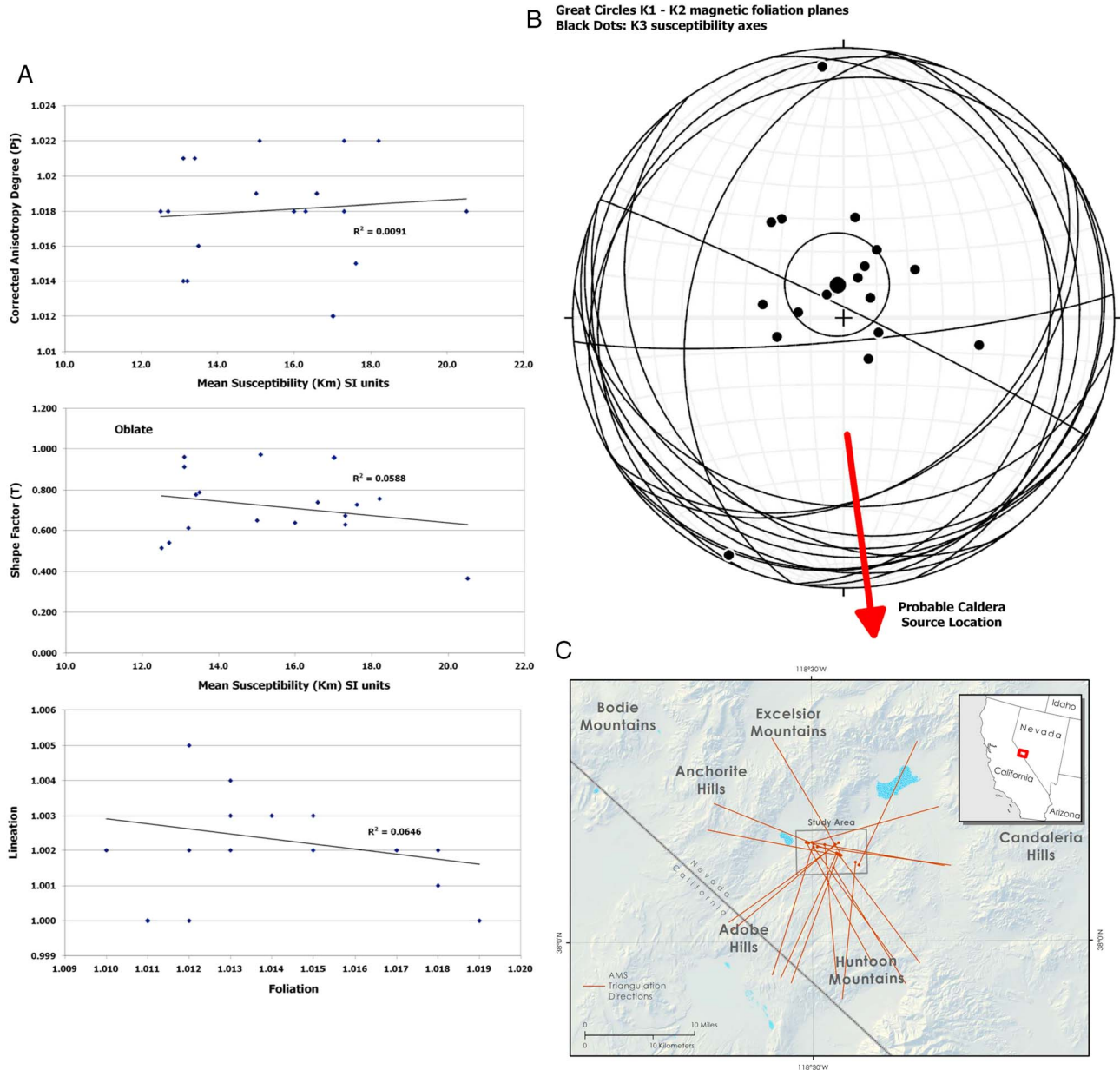# Appendix B: Anisotropy of Magnetic Susceptibility Data

Figure A2. (a) Susceptibility parameters. Upper and middle diagram: we see no correlation between the corrected anisotropy degree and the shape factor with respect to the mean susceptibility. The lower diagram indicates that all sites yield an oblate susceptibility ellipsoid, where the planar elements of the fabric dominate. (b) Lower hemisphere equal area projection of the magnetic foliation plane, K1-K2 (great circles), and normal to the magnetic foliation planes, K3 (black dots). All the AMS data have been corrected for local tilt and paleomagnetic estimated vertical axis rotation relative to the reference location in the Bodie Hills, CA. The red arrow indicates the probable direction to the source caldera (trend 178°). (c) Anisotropy of magnetic susceptibility triangulation directions. The direction is derived from the 180° bearing from the K3 susceptibility axis (i.e., normal to the magnetic foliation plane). Admittedly, the convergence is poorly defined; however, we note that (1) the thickest section of the Jack Springs Tuff outcrops in this area, and arguably we are close to the source caldera, and (2) the majority of the AMS inferred directions trend toward the southwest and southeast. We speculate that the probable source caldera is located south of the study area in the Huntoon Mountains-Queens Valley region. The high dispersion of the inferred transport directions likely reflects the interaction of the ignimbrite, and hence AMS fabrics, with the paleotopography at the time of emplacement. (d) In situ anisotropy of magnetic susceptibility data from each site in the Jack Springs Tuff. Each diagram is a lower hemisphere equal area projection of the K1, K2, and K3 susceptibility axis.
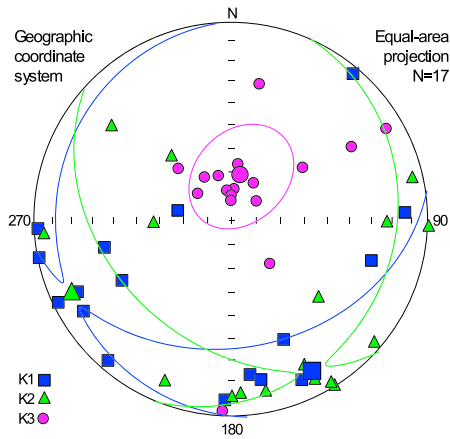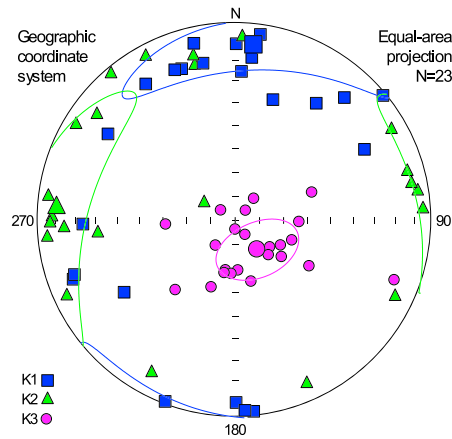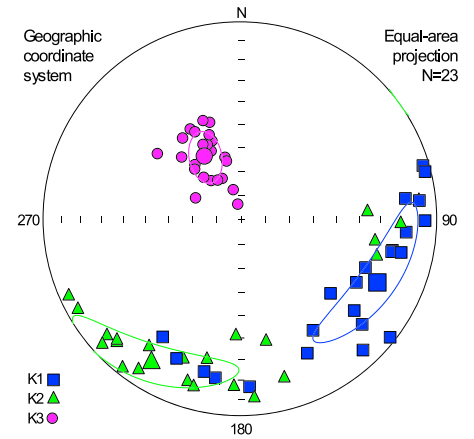
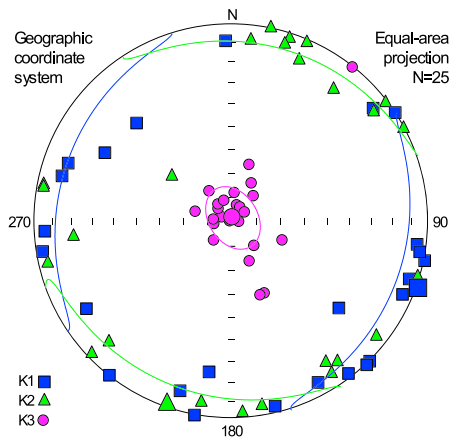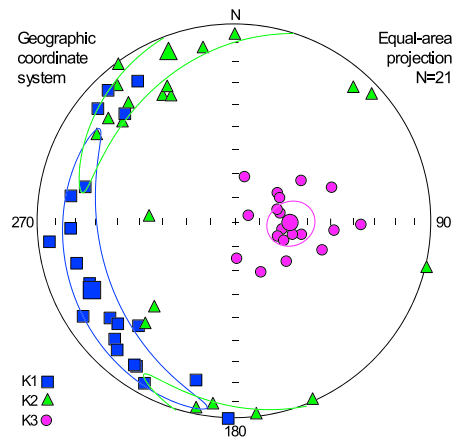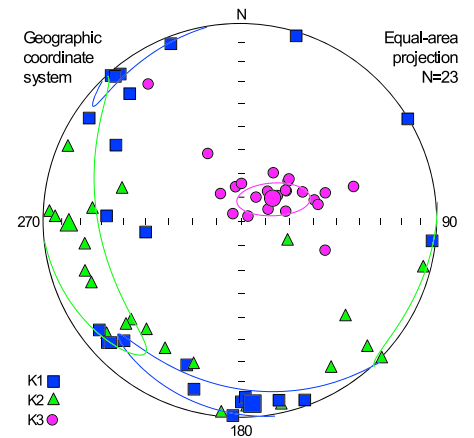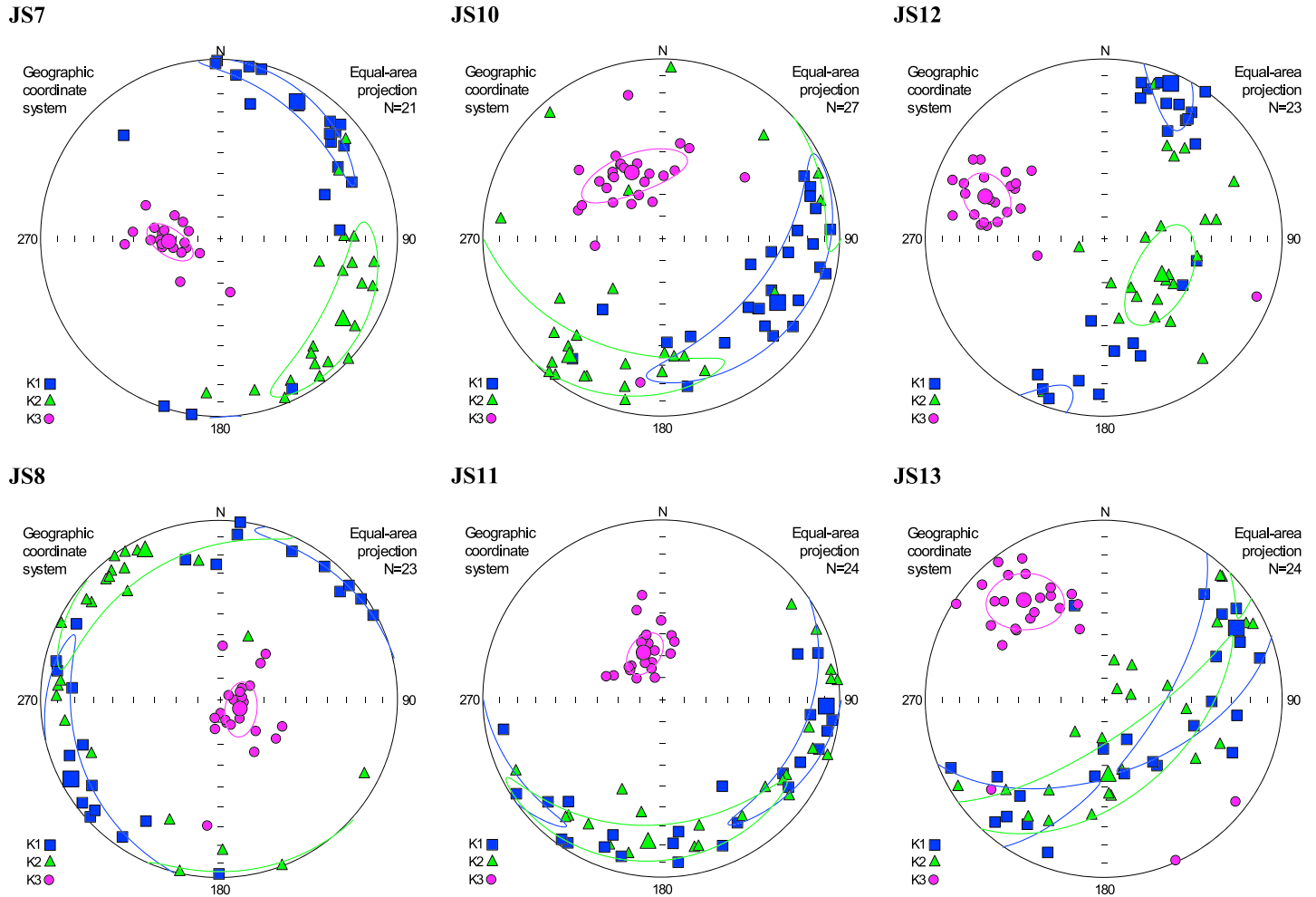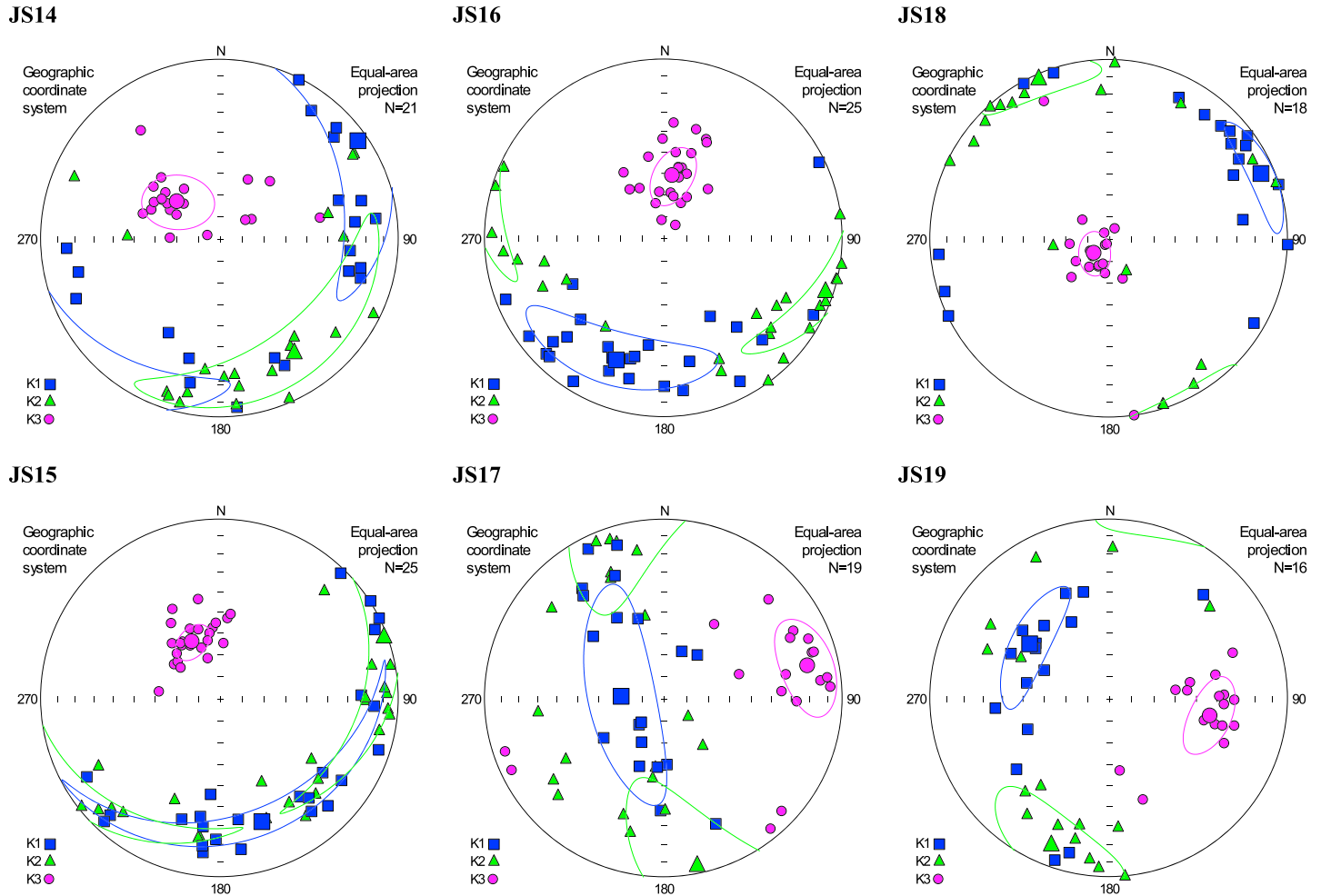**Figure A2.** (continued)

Figure A2. (continued)

Figure A2. (continued)

Appendix C

Regional aeromagnetic anomaly map and isostatic residual gravity data from the area east of Mono Lake, CA. (a) Top diagram displays the total magnetic field data for the study area. Note the rapid gradient from +250 to less than −230 nT moving north of the study area. (b) Bottom diagram: isostatic residual gravity data show a similar pattern with a rapid drop in gravity moving north from the study area. The gray dots represent gravity stations. The maps are modified from McDonell (2013) based on the data from the USGS data repository (https://pubs.usgs.gov/ds/2006/234/nv_other.htm) (Figure A3).
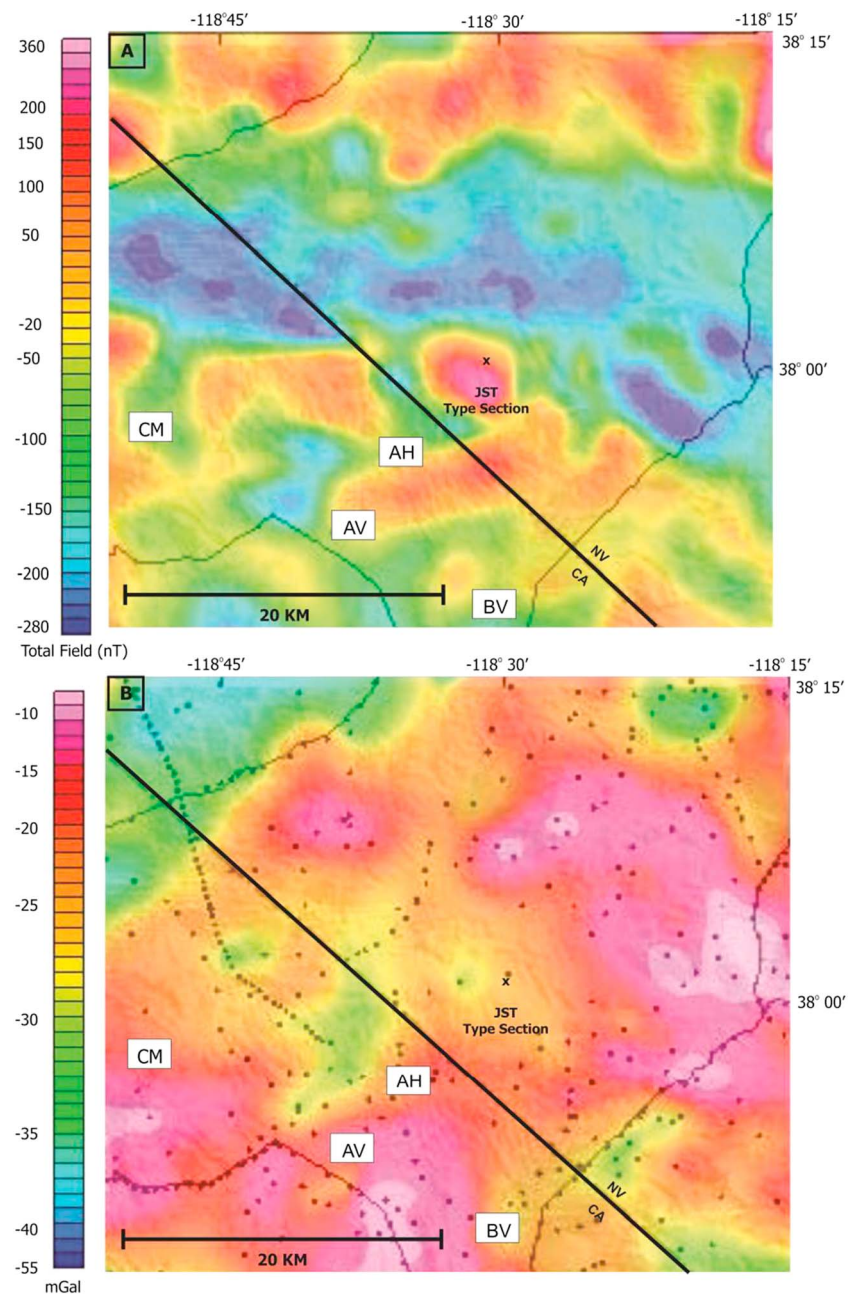
Figure A3. (a) Total magnetic field intensity in nanotesla. (b) Isostatic residual gravity data in milligals.

Appendix D: Geographic Information System Metadata

The paleomagnetic data table (Table 3) was modified in MS Excel by adding the following columns:

1. Delta Re: 25 times the delta R value representing minor axis of the error ellipse.
2. Major: a value of 500 representing the length of the major axis of the error ellipse.
3. Distance: a value of 250 representing the distance to offset the error ellipse so its base would be at the site location.

To place the ellipse so that its base would be at the site location, the ArcMap "Bearing Distance to Line" tool was used with the MS Excel table. The Bearing Field was set to the R (rotation) column in the paleomagnetic data g table. The Distance column was used for the Distance Field in the tool. The distance units were set to meters.

The endpoint coordinates of the new offset distance line was generated using the ArcMap "Add Geometry Attributes" tool. This tool added endpoint coordinates to the offset distance line feature class. The original Pmag data table was joined to the new offset distance line feature class to allow the ellipses to be developed from the endpoint of the offset line.

Error ellipses oriented to the direction of rotation were created in ArcMap using the Table to Ellipse tool and the attribute table of the offset distance line.

1. The end points were used for the *x* and *y* fields.
2. The Major column was used to set the major axis of the ellipse to a constant 500.
3. The Delta Re column was used to set the minor axis of the ellipse.
4. Distance units were set to meters.
5. The R column was used for the azimuth.
6. The spatial reference was set to NAD 1983 UTM zone 11°N.

The site locations were symbolized with a composite point and arrow symbol, with the direction of the error set to the azimuth of the rotation.

References

Akimoto, S. (1962). Magnetic properties of FeO–Fe$_2$O$_3$–TiO$_2$ system as a basis of rock magnetism. *Journal of the. Physical Society of Japan*, *17*(suppl. B1), 706–710.

Alva-Valdivia, L. M., Rosas-Elguera, J., Bravo-Medina, T., Urrutia-Fucugauchi, J., Henry, B., Caballero, C., et al. (2005). Paleomagnetic and magnetic fabric studies of the San Gaspar ignimbrite, western Mexico—Constraints on emplacement mode and source vents. *Journal of Volcanology and Geothermal Research*, *147*(1–2), 68–80. ISSN 0377-0273

Argus, D. F., & Gordon, R. G. (1991). Current Sierra Nevada-North America motion from very long baseline interferometry. *Implications for the kinematics of the western United States: Geology*, *19*, 1085–1088.

Atwater, T., & Stock, J. (1998). Pacific–North America plate tectonics of the Miocene southwestern United States—An update. *International Geology Reviews*, *40*, 375–402.

Beck, M. E. (1980). Paleomagnetic record of plate-margin tectonic processes along the western edge of North America. *Journal of Geophysical Research*, *85*, 7115–7131. https://doi.org/10.1029/JB085iB12p07115

Beck, M. E. Jr., & Burr, C. D. (1979). Paleomagnetism and tectonic significance of the Goble Volcanic Series, southwestern Washington. *Geology*, *7*, 175–179.

Bennett, R. A., Davis, J. L., & Wernicke, B. P. (1999). Present-day pattern of Cordilleran deformation in the western United States. *Geology*, *27*, 371–374.

Bennett, R. A., Wernicke, B. P., Niemi, N. A., Friedrich, A. M., & Davis, J. L. (2003). Contemporary strain rates in the northern Basin and Range Province from GPS data. *Tectonics*, *22*(2), 1008. https://doi.org/10.1029/2001TC001355

Bormann, J. M., Hammond, W. C., Kreemer, C., & Blewitt, G. (2016). Accommodation of missing shear strain in the central Walker Lane, western North America: Constraints from dense GPS measurements. *Earth and Planetary Science Letters, Volume*, *440*, 169–177. ISSN 0012-821X

Bursik, M., Renshaw, C., McCalpin, J., & Berry, M. (2003). A volcanotectonic cascade: Activation of range front faulting and eruptions by dike intrusion, Mono Basin–Long Valley Caldera, California. *Journal of Geophysical Research*, *108*(b8), 2393. https://doi.org/10.1029/2002JB002032

Byrd, J. O. D., Smith, R. B., & Geissman, J. W. (1994). The Teton fault, Wyoming: Topographic signature, neotectonics, and mechanisms of deformation. *Journal of Geophysical Research*, *99*(B10), 20,095–20,122. https://doi.org/10.1029/94JB00281

Carlson, C. W., Pluhar, C. J., Glen, J. M. G., & Farner, M. J. (2013). Kinematics of the west-central Walker Lane: Spatially and temporally variable rotations evident in the Late Miocene Stanislaus Group. *Geosphere*, *9*(6), 1530–1551. https://doi.org/10.1130/GES00955.1

Cashman, P. H., & Fontaine, S. A. (2000). Strain partitioning in the northern Walker Lane, western Nevada and north-eastern California. *Tectonophysics*, *326*, 11–130.

Chadima, M., & Hrouda, F. (2006). Remasoft 3.0—A user-friendly paleomagnetic data browser and analyzer. Travaux Géophysiques, XXVII, 20–21.

Chan, L. (1988). Apparent tectonic rotations, declination anomaly equations, and declination anomaly charts. *Journal of Geophysical Research*, *93*(B10), 12,151–12,158. https://doi.org/10.1029/JB093iB10p12151

Christensen, M. N., Gilbert, C. M., Lajoie, K. R., & Al-Rawi, Y. (1969). Geological-geophysical interpretation of Mono Basin, California-Nevada. *Journal of Geophysical Research*, *74*(22), 5221–5239.

Condie, K. C. (2016). *Earth as an Evolving Planetary System* (Third ed.p. 430). London: Academic Press. ISBN 9780128036891

Day, R., Fuller, M. D., & Schmidt, V. A. (1977). Hysteresis properties of titanomagnetites: Grain-size and compositional dependence. *Physics of the Earth and Planetary Interiors*, *13*(4), 260–267. https://doi.org/10.1016/0031-9201(77)90108-X

de Wall, H. (2000). The field dependence of AC susceptibility in titanomagnetites: Implications for the anisotropy of magnetic susceptibility. *Geophysical Research Letters*, *27*(16), 2409–2411. https://doi.org/10.1029/2000GL008515

Demarest, H. H. (1983). Error analysis of the determination of tectonic rotation from paleomagnetic data. *Journal of Geophysical Research*, *88*, 4321–4328. https://doi.org/10.1029/JB088iB05p04321

Dixon, T. H., Miller, M., Farina, F., Wang, H., & Johnson, D. (2000). Present-day motion of the Sierra Nevada block and some tectonic implications for the Basin and Range Province, North American Cordillera. *Tectonics*, *19*(1), 1–24. https://doi.org/10.1029/1998TC001088

Dixon, T. H., Norabuena, E., & Hotaling, L. (2003). Paleoseismology and Global Positioning System: Earthquake-cycle effects and geodetic versus geologic fault slip rates in the Eastern California shear zone. *Geology*, *31*(1), 55–58. https://doi.org/10.1130/0091-7613(2003)031<0055:PAGPSE>2.0.CO;2

Dixon, T. H., Robaudo, S., Lee, J., & Reheis, M. C. (1995). Constraints on present-day Basin and Range deformation from space geodesy. *Tectonics*, *14*(4), 755–772. https://doi.org/10.1029/95TC00931

Dokka, R. K., & Travis, C. J. (1991). Late Cenozoic strike-slip faulting in the Mojave desert, California. *Tectonics, Washington*, *9*, 311–340.

Dokka, R. K., & Travis, C. J. (1996). Role of the Eastern California shear zone in accommodating Pacific-North American plate motion. *Geophysical Research Letters*, *17*, 1323–1326.

Dunlop, D. J. (2002). Theory and application of the Day plot (Mrs/Ms versus Hcr/Hc) 1, Theoretical curves and tests using titanomagnetite data. *Journal of Geophysical Research*, *107*(B3), 2056. https://doi.org/10.1029/2001JB000486

Dunlop, D. J., & Özdemir, O. (1997). *Rock Magnetism: Fundamentals and Frontiers, Cambridge Studies in Magnetism*. 3, (p. 573). New York: Cambridge University Press.

Ellwood, B. B. (1982). Estimates of flow direction for calc-alkaline welded tuffs and paleomagnetic data reliability from anisotropy of magnetic susceptibility measurements: Central San Juan Mountains, southwest Colorado. *Earth and Planetary Science Letters*, *59*(2), 303–314. https://doi.org/10.1016/0012-821X(82)90133-9

Faulds, J. E., & Henry, C. D. (2008). Tectonic influences on the spatial and temporal evolution of the Walker Lane: An incipient transform fault along the evolving Pacific–North American plate boundary, in Spencer, J.E., and Titley, S.R., eds. *Ores and orogenesis: Circum-Pacific tectonics, geologic evolution, and ore deposits: Arizona Geological Society Digest*, *22*, 437–470.

Faulds, J. E., & Varga, R. J. (1998). The role of accommodation zones and transfer zones in the regional segmentation of extended terranes. In J. E. Faulds & J. Stewart (Eds.), *The regional segmentation of the Basin and Range Province, Geological Society of America Special Papers* (Vol. 323, pp. 1–45).

Ferranti, L., & Oldow, J. S. (2005). Active displacement transfer and finite flattening on curved faults, central Walker Lane, Western Great Basin, Nevada. Geological Society of America Penrose Conference Kinematics and Geodynamics of Intraplate Dextral Shear in Eastern California and Western Nevada, 21–26 April, Mammoth Lakes, California.

Ferranti, L., Oldow, J. S., Geissman, J. W., & Neil, M. M. (2009). Flattening strain during coordinated slip on a curved fault array, Rhodes Salt Marsh extensional basin, central Walker Lane, west-central Nevada, in Oldow, J.S., and Cashman, P.H., eds., Late Cenozoic structural and evolution of the Great Basin–Sierra Nevada transition transition: Geological Society of America Special Paper 447, p. 189–214. https://doi.org/10.1130/2009.2447(11)

Fisher, R. A. (1953). Dispersion on a sphere. *Proceedings of the Royal Society of London. Series A*, *217*(1130), 295–305. https://doi.org/10.1098/rspa.1953.0064

Foy, T., Frankel, L. K., Lifton, Z., Johnson, C., & Caffee, M. (2012). Distributed extensional deformation in a zone of right-lateral shear: Implications for geodetic versus geologic rates of deformation in the eastern California shear zone-Walker Lane. *Tectonics*, *31*, TC4008. https://doi.org/10.1029/2011TC002930

Frankel, K. L., Dolan, J. F., Ganev, P., & Finkel, R. C. (2011). Spatial and temporal constancy of seismic strain release along an evolving segment of the Pacic-North America plate boundary. *Earth and Planetary Science Letters*, *304*, 565–576. https://doi.org/10.1016/j.epsl.2011.02.034

Gattacceca, J., Deino, A., Rizzo, R., Jones, D. S., Henry, B., Beaudoin, B., & Vadeboin, F. (2007). Miocene rotation of Sardinia: New paleomagnetic and geochronological constraints and geodynamic implications. *Earth and Planetary Science Letters*, *258*(3–4), 359–377. ISSN 0012-821X

Geissman, J. W., Callian, J. T., Oldow, J. S., & Humphries, S. E. (1984). Paleomagnetic assessment of oroflexural deformation in west-central Nevada and significance for emplacement of allochthonous assemblages. *Tectonics*, *3*(2), 179–200. https://doi.org/10.1029/TC003i002p00179

Gilbert, C. M., Christensen, M. N., Al Rawi, Y., & Lajoie, K. R. (1968). Structural and volcanic history of Mono Basin. *California-Nevada: Geological Society of America Memoirs*, *116*, 275–329.

Gillett, S. L., & Vanalstine, D. R. (1982). Remagnetization and tectonic rotation of Upper Precambrian and Lower Paleozoic strata from the Desert Range, southern Nevada. *Journal of Geophysical Research*, *87*(B13), 10,929–10,953. https://doi.org/10.1029/JB087iB13p10929

Gledhill, T., Pluhar, C. J., Johnson, S. A., Lindeman, J. R., & Petronis, M. S. (2016). A kinematic model for vertical axis rotation within the Mina Deflection of the Walker Lane, American Geophysical Union, Fall Meeting, Abstract GP31B-1300.

Grondin, D. P., Petronis, M., Lindline, J., & Romero, B. P. (2016). Vertical axis clockwise rotation of fault blocks in the Eastern Mono Basin, California And Nevada, Session No. 347--Booth# 459, Geological Society of America Abstracts with Programs. Vol. 48, No. 7. https://doi.org/10.1130/abs/2016AM-286303

Grondin, D. P., & Petronis, M. S. (2016). Timing of intercontinental deformation across the Eastern Mono Basin, California and Nevada, Rocky Mountain Section—68th Annual Meeting. *Geological Society of America Abstracts with Programs*. *48*(6). https://doi.org/10.1130/abs/2016RM-276135

Hammond, W. C., Blewitt, G., & Kreemer, C. (2011). Block modeling of crustal deformation of the northern Walker Lane and Basin and Range from GPS velocities. *Journal of Geophysical Research*, *116*, B04402. https://doi.org/10.1029/2010JB007817

Hardyman, R. F. (1984). Strike-slip, normal, and detachment faults in the northern Gillis Range, Walker Lane of west central Nevada. In J. Lintz, Jr. (Ed.), *Western Geologic Excursions, Volume 4: Geological Society of America Annual Meeting Guidebook* (pp. 184–203). Reno, Nevada: Mackay School of Mines.

Hrouda, F., Putiš, M., & Madarás, J. (2002). The Alpine overprints of the magnetic fabrics in the basement and cover rocks of the Veporic Unit (Western Carpathians, Slovakia). *Tectonophysics*, *359*, 271–288.

Hudson, M. R., & Geissman, J. W. (1985). Paleomagnetic and structural evidence for middle Tertiary counterclockwise rotation in the Dixie Valley region, west-central Nevada. *Geology*, *15*, 638–642. 1987

Hudson, M. R., Rosenbaum, J. G., Gromme, C. S., Scott, R. B., & Rowley, P. D. (1998). Paleomagnetic evidence for counterclockwise rotation in a broad sinistral shear zone, Basin and Range Province, southeastern Nevada and southwestern Utah: Geological Society of America Special Paper 323, p. 149–181.

Hudson, M. R., Sawyer, D. A., & Warren, R. G. (1994). Paleomagnetism and rotation constraints for the middle Miocene southwestern Nevada volcanic field. *Tectonics*, *13*(2), 258–277.

Jackson, M., Moskowitz, B., Rosenbaum, J., & Kissel, C. (1998). Field dependence of AC susceptibility in titanomagnetite. *Earth and Planetary Science Letters*, *157*(3-4), 129–139. https://doi.org/10.1016/S0012-821X(98)00032-6

Jackson, M., & Swanson-Hysell, N. (2012). Rock magnetism of remagnetized carbonate rocks: Another look. In R. D. Elmore, A. R. Muxworthy, M. M. Aldana, & M. Mena (Eds.), *Remagnetization and Chemical Alteration of Sedimentary Rocks* (Vol. 371, pp. 229–251). Geological Society, London, Special Publications. https://doi.org/10.1144/SP371.3

Janecke, S. U., Geissman, J. W., & Bruhn, R. L. (1991). Localized rotation during Paleogene extension in east central Idaho: Paleomagnetic and geologic evidence. *Tectonics*, *10*(2), 403–432.

Jayko, A. S., & Bursik, M. (2012). Active transtensional intracontinental basins: Walker Lane in the western Great Basin. In C. Busby and A. Azor (Eds.), *Tectonics of Sedimentary Basins*. https://doi.org/10.1002/9781444347166.ch11

John, D. A., du Bray, E. A., Blakely, R. J., Fleck, R. J., Vikre, P. G., Box, S. E., & Moring, B. C. (2012). Miocene magmatism in the Bodie Hills volcanic field, California and Nevada: A long-lived eruptive center in the southern segment of the ancestral Cascades arc. *Geosphere*, *8*, 44–97. https://doi.org/10.1130/GES00674.1

John, D. A., du Bray, E. A., Box, S. E., Vikre, P. G., Rytuba, J. J., Fleck, R. J., & Moring, B. C. (2015). Geologic map of the Bodie Hills, California and Nevada, Pamphlet to accompany, Scientific Investigations Map 3318, U.S. Department of the Interior, U.S. Geological Survey.

Johnson, S., Pluhar, C., & Lindeman, J. (2014). Paleomagnetism and lithostratigraphy of the Miocene Tuff of Huntoon Creek Type Section, American Geophysical Union, Fall Meeting, abstract #GP21A-3651.

Jones, C. H., Farmer, G. L., & Unruh, J. (2004). Tectonics of Pliocene removal of lithosphere of the Sierra Nevada. *California: Geological Society of America Bulletin*, *116*, 1408–1422. https://doi.org/10.1130/B25397.1

Jelínek, V. (1981). Characterization of the m agnetic fabric of rocks. *Tectonophysics*, *79*, T63–T67.

Kamerling, M. J., & Luyendyk, B. P. (1985). Paleomagnetism and Neogene tectonics of the northern Channel Islands, California. *Journal of Geophysical Research*, *90*(B14), 12,485–12,502. https://doi.org/10.1029/JB090iB14p12485

King, N. M., Hillhouse, J. W., Grommé, S., Hausback, B. P., & Pluhar, C. J. (2007). Stratigraphy, paleomagnetism and anisotropy of magnetic susceptibility of the Miocene Stanislaus Group, central Sierra Nevada and Sweetwater Mountains, California and Nevada. *Geosphere*, *3*(6), 646–666. https://doi.org/10.1130/GES00132.1

Kirshvinck, J. L. (1980). The least-squares line and plane and the analysis of paleomagnetic data. *Geophysical Journal International*, *62*, 699–718.

Kleinhampl, F. J., Davis, W. E., Silberman, M. L., Chesterman, C. W., Chapman, R. H., & Gray, C. H. Jr. (1975). *Aeromagnetic and Limited Gravity Studies and Generalized Geology of the Bodie Hills Region, Nevada and California*. Reston, VA: US Geological Survey. 8755–531x

Knight, M. D., Walker, G. P. L., Ellwood, B. B., & Diehl, J. F. (1986). Stratigraphy, paleomagnetism, and magnetic fabric of the Toba Tuffs: Constraints on the sources and eruptive styles. *Journal of Geophysical Research*, *91*(B10), 10,355–10,382. https://doi.org/10.1029/JB091iB10p10355

Kreemer, C., Blewitt, G., & Hammond, W. C. (2009). Geodetic constraints on contemporary deformation in the northern Walker Lane: 2. Velocity and strain rate tensor analysis. In J. S. Oldow & P. H. Cashman (Eds.), *Late Cenozoic Structural and Evolution of the Great Basin–Sierra Nevada Transition* (pp. 17–31). Colorado, USA, Special Paper 447: Geological Society of America. https://doi.org/10.1130/2009.2447(02)

Kuiper, K. F., Deino, A., Hilgen, F. J., Krijgsman, W., Renne, P. R., & Wijbrans, J. R. (2008). Synchronizing rock clocks of Earth history. *Science*, *320*, 500–504.

Lamarche, G., & Frogatt, P. C. (1993). New eruptive vents for the Whakamaru ignimbrite (Taupo volcanic zone) identified from magnetic fabric study. *New Zealand Journal of Geology and Geophysics*, *36*(2), 213–222. https://doi.org/10.1080/00288306.1993.9514569

Lee, J., Garwood, J., Stockli, D., & Gosse, J. (2009). Quaternary faulting in Queen Valley, California-Nevada: Implications for kinematics of fault slip transfer in the Eastern California Shear Zone-Walker Lane Belt. *Geological Society of America Bulletin*, *121*, 599–614. https://doi.org/10.1130/B26352.1

Lee, J., Pencer, J., & Owens, L. (2001). Holocene slip rates along the Owens Valley fault, California: Implications for the recent evolution of the eastern California shear zone. *Geology*, *29*, 819–822.

Lee, J., Stockli, D., Schroeder, J., Tincher, C., Bradley, D., & Owen, L. (2005). Fault slip transfer in the eastern California Shear Zone/Walker Lane Belt, with field guide. In J. Lee, D. Stockli, C. D. Henry & T. H. Dixon (Eds.), *Penrose Conference: Kinematics and Geodynamics of Intraplate Dextral Shear in Eastern California and Western Nevada* (pp. 22–46). Mammoth Lakes: Geological Society of America.

Lindeman, J. R., Pluhar, C. J., & Farner, M. J. (2013). Post-middle Miocene Tuffs: Vertical axis rotation from paleomagnetic analysis within Bodie Hills and Mono Basin, Eastern California and Western Nevada. American Geophysical Union, Fall Meeting, abstract #GP41A-1113.

Locke, A., Billingsly, P. R., & Mayo, E. B. (1940). Sierra Nevada tectonic patterns. *Geological Society of America Bulletin*, *51*(4), 513–539. https://doi.org/10.1130/GSAB-51-513

Luyendyk, B. P., Kamerling, M. J., Terres, R. R., & Hornafius, J. S. (1985). Simple shear of Southern California during Miocene time suggested by paleomagnetic declinations. *Journal of Geophysical Research*, *90*, 12,454–12,466.

MacDonald, W. D., & Palmer, H. C. (1990). Flow directions in ashflow tufts: a comparison of geological and magnetic susceptibility measurements, Tshirege member (upper Bandelier Tuff), Valles caldera New Mexico, USA. *Bulletin of Volcanology*, *53*, 45–59.

Malservisi, R., Furlong, K. P., & Dixon, T. H. (2003). Influence of the earthquake cycle and lithosphere rheology on the dynamics of the eastern California shear zone. *Geophysical Research Letters*, *28*(14), GL013311. https://doi.org/10.1029/2001GL013311

McCaffrey, R. (2002). Crustal block rotations and plate coupling. In S. Stein & J. Freymueller (Eds.), *Plate Boundary Zones, AGU Geodynamics Series* (Vol. 30, pp. 101–122).

McDonell, A. P. (2013). *Geophysical Expression of the Northern Part of the Mono-Inyo Volcanic Chain, Mono Basin, California*, Masters of Science Thesis (p. 89). CA: San Jose State University.

McKenzie, D., & Jackson, J. (1986). A block model of distributed deformation by faulting. *Journal of the Geological Society of London*, *143*, 349–353.

McKenzie, D. P., & Jackson, J. A. (1983). The relationship between strain rates, crustal thickening, palaeomagnetism, finite strain and fault movements within a deforming zone. *Earth and Planetary Science Letters*, *65*(1), 182–202. https://doi.org/10.1016/0012-821X(83)90198-X

Miller, M. M., Johnson, D. J., Dixon, T. H., & Dokka, R. K. (2001). Refined kinematics of the Eastern California shear zone from GPS observations, 1993–1998. *Journal of Geophysical Research*, *106*, 2245–2263.

Min, K., Mundil, R., Renne, P. L., & Ludwig, K. R. (2000). A test for systematic errors in $^{40}Ar/^{39}Ar$ geochronology through comparison with U/Pb analysis of a 1.1-Ga rhyolite. *Geochimica et Cosmochimica Acta*, *64*(1), 73–98.

Minster, J. B., & Jordan, T. H. (1987). Vector constraints on western United States deformation from space geodesy, neotectonics, and plate motions. *Journal of Geophysical Research*, *92*, 4798–4804. https://doi.org/10.1029/JB092iB06p04798

Moskowitz, B. M., Frankel, R. B., & Bazylinski, D. A. (1993). Rock magnetic criteria for the detection of biogenic magnetite. *Earth and Planetary Science Letters*, *120*(3-4), 283–300. https://doi.org/10.1016/0012-821X(93)90245-5

Nagorsen-Rinkel, S., Lee, J., & Calvert, A. (2013). Pliocene sinistral slip across the Adobe Hills, eastern California-western Nevada: Kinematics of fault slip transfer across the Mina Deflection. *Geosphere*, *9*(1), 37–53. https://doi.org/10.1130/GES00825.1

Oldow, J. S. (1992a). Late Cenozoic displacement partitioning in the northwestern Great Basin. In S. D. Graig (Ed.), *Structure, Tectonics, and Mineralization of the Walker Lane* (pp. 17–52). Reno, Nevada: Geological Society of Nevada Walker Lane Symposium Proceedings Volume.

Oldow, J. S. (1992b). Late Cenozoic displacement partitioning in the northwestern Great Basin. In S. D. Graig (Ed.), (pp. 7–52). Reno, Nevada: Geological Society of Nevada, Walker Lane Symposium Proceedings Volume.

Oldow, J. S. (2003). Active transtensional boundary zone between the western Great Basin and Sierra Nevada block, western US Cordillera. *Geology*, *31*(12), 1033–1036. https://doi.org/10.1130/G19838.1

Oldow, J. S., Aiken, C. L. V., Hare, J. L., Ferguson, J. F., & Hardyman, R. F. (2001). Active displacement transfer and differential block motion within the central Walker Lane, western Great Basin. *Geology*, *29*(1), 19–22.

Oldow, J. S., Elias, E. A., Ferranti, L., McClelland, W. C., & McIntosh, W. C. (2009). Late Miocene to Pliocene synextensional deposition in fault-bound basins within the upper plate of the western Silver Peak - Lone Mountain extensional complex, west-central Nevada. In J. S. Oldow & P. H. Cashman (Eds.), *Late Cenozoic evolution of the western Great Basin, Geological Society of America Special Paper* (Vol. 447, pp. 275–312).

Oldow, J. S., Geissman, J. W., & Stockli, D. F. (2008). Evolution and strain reorganization within late Neogene structural stepovers linking the central Walker Lane and northern Eastern California Shear Zone, western Great Basin. *International Geology Review*, *50*, 270–290. https://doi.org/10.2747/0020-6814.50.3.270

Oldow, J. S., Kohler, G., & Donelick, R. A. (1994). Low-angle displacement transfer system linking the Furnace Creek and Walker Lane fault zones, west-central Nevada. *Geology*, *22*, 637–640.

Ort, M. H. (1993). Eruptive processes and caldera formation in a nested downsag-collapse caldera: Cerro Pardzos, central Andes Mountains. *Journal of Volcanology and Geothermal Research*, *56*(3), 221–252. https://doi.org/10.1016/0377-0273(93)90018-M

Ort, M. H., Rosi, M., & Anderson, C. D. (1999). Correlation of deposits and vent locations of the proximal Campanian Ignimbrite deposits, Campi Flegrei, Italy, based on natural remanent magnetization and anisotropy of magnetic susceptibility characteristics. *Journal of Volcanology and Geothermal Research*, *91*(2–4), 167–178. https://doi.org/10.1016/S0377-0273(99)00034-7

Özdemir, Ö., & Dunlop, D. J. (1997). Effect of crystal defects and internal stress on the domain structure and magnetic properties of magnetite. *Journal of Geophysical Research*, *102*(20), 211–220. 224

Özdemir, Ö., Dunlop, D. J., & Moskowitz, B. M. (1993). The effect of oxidation on the Verwey transition in magnetite. *Geophysical Research Letters*, *20*(16). https://doi.org/10.1029/93GL01483

Özdemir, Ö., & O'Reilly, W. (1981). High-temperature hysteresis and other magnetic properties of synthetic monodomain titanomagne-tites. *Physics of the Earth and Planetary Interiors*, *25*(4), 406–418. ISSN 0031–9201

Özdemir, Ö., & O'Reilly, W. (1982). Magnetic hysteresis properties of synthetic monodomain titanomaghemites. *Earth and Planetary Science Letters*, *57*(2), 437–447. ISSN 0012-821X

Pakiser, L. C., Press, F., & Kane, M. F. (1960). Geophysical investigation of Mono Basin. *California: Bulletin of the Geological Society of America*, *71*, 415–448.

Palmer, H. C., MacDonald, W. D., & Hayatsu, A. (1991). Magnetic, structural and geochronological evidence bearing on volcanic sources and Oligocene deformation of ash flow tuffs, northeast Nevada. *Journal of Geophysical Research*, *96*(B2), 2185–2202. https://doi.org/10.1029/90JB02224

Parry, L. G. (1982). Magnetization of immobilized particle dispersions with two distinct particle sizes. *Physics of the Earth and Planetary Interiors*, *28*(3), 230–241. ISSN 0031–9201

Petronis, M. S., Brister, A. R., Rapprich, V., van Wyk de Vries, B., Lindline, J., & Mišurec, J. (2015). Emplacement history of the Trosky basanitic volcano (Czech Republic): Paleomagnetic, rock magnetic, petrologic, and anisotropy of magnetic susceptibility evidence for lingering growth of a monogenetic volcano. *Journal of Geosciences*, *60*(3), 129–147. http://doi.org/10.3190/jgeosci.196

Petronis, M. S., Geissman, J. W., Oldow, J. S., & McIntosh, W. C. (2002). Paleomagnetic and $^{40}Ar/^{39}Ar$ geochronologic data bearing on the structural history of the Silver Peak Range, west-central Nevada. *Geological Society of America Bulletin*, *114*, 1108–1130.

Petronis, M. S., Geissman, J. W., Oldow, J. S., & McIntosh, W. C. (2007). Tectonism of the southern Silver Peak Range: Paleomagnetic and geochronologic data bearing on the Miocene development of a regional extensional complex, central Walker Lane, Nevada. In A. B. Till, S. M. Roeske, J. C. Sample, & D. A. Foster (Eds.), *Exhumation Associated With Continental Strike-Slip Systems* (pp. 81–106). Colorado, USA, Spec Pap 434: Geol Soc Am.

Petronis, M. S., Geissman, J. W., Oldow, J. S., & McIntosh, W. C. (2009). Late Miocene to Pliocene vertical-axis rotation attending development of the Silver Peak–Line Mountain displacement transfer zone, west-central Nevada. In J. S. Oldow, & P. H. Cashman (Eds.), *Late Cenozoic Structure and Evolution of the Great Basin–Sierra Nevada Transition* (pp. 215–254). Colorado, USA, Special Paper 447: Geological Society of America. https://doi.org/10.1130/2009.2447(12)

Petronis, M. S., Grondin, D., Castillo, G., Shields, S., Lindline, J., Romero, B., & Pluhar, C. J. (2016). The eastern Mono Basin transtensional zone: New paleomagnetic and $^{40}Ar/^{39}Ar$ data bearing on the timing and extent of vertical axis rotation associated with intercontinental deformation, GP31B-1302, Annual American Geophysical Union Meeting in San Francisco, CA (December 12th – 16th December 2016).

Petronis, M. S., Holm, D. K., Geissman, J. W., Arnold, B. J., & Hacker, D. B. (2014). Paleomagnetic results from the Eastern Caliente-Enterprise Zone, SW Utah: Implications for initiation of a major Miocene transfer zone. *Geosphere*, *10*(3), 534–563. https://doi.org/10.1130/GES00834

Reheis, M. C., & Sawyer, T. L. (1997). Late Cenozoic history and slip rates of the Fish Lake Valley, Emigrant Peak, and Deep Springs fault zone, Nevada and California. *Geological Society of America Bulletin*, *109*, 280–299.

Reynolds, R. L. (1977). Paleomagnetism of welded tuffs of the Yellowstone Group. *Journal of Geophysical Research*, *82*(26), 3677–3693. https://doi.org/10.1029/JB082i026p03677

Roberts, C. W., & Jachens, R. C. (1999). Preliminary aeromagnetic anomaly map of California: U.S. Geological Survey Open-File Report 99–440, 14 p.

Ron, H., Freund, R., Garfunkel, Z., & Nur, A. (1984). Block rotation by strike slip faulting: Structural and paleomagnetic evidence. *Journal of Geophysical Research*, *89*, 6256–6270.

Rood, D. H., Burbank, D. W., Herman, S. W., & Bogue, S. (2011). Rates and timing of vertical-axis block rotations across the central Sierra Nevada–Walker Lane transition in the Bodie Hills, California/Nevada. *Tectonics*, *30*, TC5013. https://doi.org/10.1029/2010TC002754

Rowan, C. J., & Roberts, A. P. (2008). Widespread remagnetizations and a new view of tectonic rotations within the Australia-Pacific plate boundary zone, New Zealand. *Journal of Geophysical Research*, *113*, B03103. https://doi.org/10.1029/2006JB004594

Ryall, A. S., & Priestly, K. (1975). Seismicity, secular strain, and maximum magnitude in the Excelsior Mountains area, western Nevada and eastern California. *Geological Society of America Bulletin*, *86*(11), 1585–1592. https://doi.org/10.1130/0016-7606(1975)86<1585:SSSAMM>2.0.CO;2

Seaman, S. J., McIntosh, W. C., Geissman, J. W., Williams, M. L., & Elston, W. E. (1991). Magnetic fabrics of the Blood Canyon and Shelley Peak Tuffs, southwestern New Mexico: Implications for emplacement and alteration processes. *Bulletin of Volcanology*, *53*, 469–476.

Sigurdsson, H., Houghton, B., Rymer, H., Stix, J., & McNutt, S. (1999). *Encyclopedia of Volcanoes* (1417 pp.). Academic Press. ISBN 10: 012643140X ISBN 13: 9780126431407

Simpson, R. W., & Cox, A. (1977). Paleomagnetic evidence for tectonic rotation of the Oregon Coast Range. *Geology*, *5*(10), 585–589. https://doi.org/10.1130/0091-7613(1977)5<585:PEFTRO>2.0.CO;2

Smirnov, A. V. (2009). Grain size dependence of low-temperature remanent magnetization in natural and synthetic magnetite: Experimental study. *Earth Planets and Space*, *61*(1), 119–124. https://doi.org/10.1186/BF03352891

Sonder, L. J., Jones, C. H., Salyards, S. L., & Murphy, K. M. (1994). Vertical axis rotations in the Las Vegas Valley shear zone, southern Nevada: Paleomagnetic constraints on kinematics and dynamics of block rotations. *Tectonics*, *13*, 769–788. https://doi.org/10.1029/94TC00352

Sprain, C. J., Feinberg, J. M., Renne, P. R., & Jackson, M. (2016). Importance of titanohematite in detrital remanent magnetizations of strata spanning the Cretaceous-Paleogene boundary, Hell Creek region, Montana. *Geochemistry, Geophysics, Geosystems*, *17*, 660–678. https://doi.org/10.1002/2015GC006191

Stewart, J. H. (1980). *Geology of Nevada: Reno*, (p. 136). Nevada Bureau of Mines and Geology: Nevada.

Stewart, J. H. (1981). Geology of the Basalt quadrangle, Mineral County, Nevada, 1:24,000. *U.S. Geological Survey Open File Report*, 82–369.

Stewart, J. H. (1984). Geologic map of the Teels Marsh Quadrangle, Mineral County, Nevada: U.S. Geological Survey Open-File Report 84–504, 1:24,000.

Stewart, J. H. (1988). Tectonics of the Walker Lane belt, western Great Basin: Mesozoic and Cenozoic deformation in a shear zone. In W. G. Ernest (Ed.), *Metamorphism and Crustal Evolution of the Western United States* (pp. 681–713). Englewood Cliffs, New Jersey: Prentice-Hall.

Stewart, J. H., & Diamond, D. S. (1990). Changing patterns of extensional tectonics; Overprinting of the basins of the middle and upper Miocene Esmeralda Formation in western Nevada by younger structural basins. In B. P. Wernicke (Ed.), *Basin and Range Extensional Tectonics Near the Latitude of Las Vegas, Nevada* (Vol. 176, pp. 447–476). Colorado, USA: Geological Society of America Memoir.

Stockli, D. F. (1999). Regional timing and spatial distribution of Miocene extension in the northern Basin and Range Province. Ph.D. thesis, Stanford University, 239 p.

Surpless, B. E. (2008). Modern strain localization in the central Walker Lane, western United States: Implications for the evolution of intraplate deformation in transtensional settings. *Tectonophysics*, *457*, 239–253. https://doi.org/10.1016/j.tecto.2008.07.001

Sussman, A., Lewis, C., Soto, R., & Goteti, R. (2006). Vertical axis rotations associated with relay ramps in the Rio Grande rift, New Mexico. *Geological Society of America Abstracts with Programs*, *38*, 417.

Tarling, D. H., & Hrouda, F. (1993). *The Magnetic Anisotropy of Rocks*, (p. 217). London: Chapman and Hall Publishers.

Taylor, J. R. (1982). *An Introduction to Error Analysis: The Study of Uncertainties in Physical Measurements*, (p. 270). Mill Valley, Calif: Univ. Sci. Books.

Thatcher, W., Foulger, G., Julian, B., Svarc, J., Quility, E., & Bawden, G. (1999). Present-day deformation across the Basin and Range Province, western U.S. *Science*, *283*(5408), 1714–1718. https://doi.org/10.1126/science.283.5408.1714

Tincher, C. R., & Stockli, D. (2005). Geological Society of America Penrose Conference kinematics and geodynamics of intraplate dextral shear in Eastern California and Western Nevada, 21–26 April, Mammoth Lakes, California.

Verwey, E. J., Haayman, P. W., & Romeijn, F. C. (1947). Physical properties and cation arrangements of oxides with spinel structure II. Electronic conductivity. *The Journal of Chemical Physics*, *15*(4), 181–187. https://doi.org/10.1063/1.1746466

Verwey, E. J. W. (1939). Electronic conduction of magnetite (Fe3O4) and its transition point at low temperatures. *Nature*, *144*, 327–328.

Wallace, R. E. (1984). Patterns and timing of late Quaternary faulting in the Great Basin Province and relation to some regional tectonic features. *Journal of Geophysical Research*, *89*, 5763–5769.

Wells, R. E., & Hillhouse, J. W. (1989). Paleomagnetism and tectonic rotation of the lower Miocene Peach Springs Tuff-Colorado Plateau, Arizona to Barstow, California. *Geological Society of America Bulletin*, *101*(6), 846–863. https://doi.org/10.1130/0016-7606(1989)101<0846:PATROT>2.3.CO;2

Wesnousky, S. G. (2005). Active faulting in the Walker Lane. *Tectonics*, *24*, TC3009. https://doi.org/10.1029/2004TC001645

Wesnousky, S. G., Bormann, J. M., Kreemer, C., Hammond, W. C., & Brune, J. N. (2012). Neotectonics, geodesy, and seismic hazard in the northern Walker Lane of Western North America: Thirty kilometers of crustal shear and no strike-slip? *Earth and Planetary Science Letters*, *329–330*, 133–140. https://doi.org/10.1016/j.epsl.2012.02.018

Wolff, J. A., Ellwood, B. B., & Sachs, S. D. (1989). Anisotropy of magnetic susceptibility in welded tuffs: application to a welded-tuff dyke in the Tertiary Trans-Pecos Texas Volcanic Province, USA. *Bulletin of Volcanology*, *51*(4), 299–310. https://doi.org/10.1007/BF01073518

Zijderveld, J. D. A. (1967). A.C. Demagnetization of rocks: Analysis of results. In D. W. Collinson, K. M. Creer, & S. K. Runcorn (Eds.), *Methods in Paleomagnetism* (pp. 254–286). Amsterdam: Elsevier.